2008

# Feasibility study of high altitude atmospheric launchers to orbit

Anna Rapo
*San Jose State University*

WORKS CITED

Anderson, John D., Jr. *Fundamentals of Aerodynamics*. San Francisco: McGraw-Hill Higher Education, 2001. Print.

---. *Hypersonic and High-Temperature Gas Dynamics*. Reston: AIAA Education Series, 2006. Print.

---. *Introduction to Flight*. San Francisco: McGraw-Hill Higher Education, 2005. Print.

Collie, C. H. *Kinetic Theory and Entropy*. New York: Longman Inc., 1982. Print.

HobbySpace. "Near Space: The Shore of our New Ocean." *HobbySpace.com*. Space-H Services, 2007. Web. 14 Mar. 2008. <http://www.hobbyspace.com/NearSpace/index.html>.

Loeb, Leonard B. *The Kinetic Theory of Gases*. New York: Dover Publications, 1961. Print.

Parker, Randall. "Aircraft and Space Shuttle Accident Rates." *FuturePundit.com*. FuturePundit, 5 Feb. 2003. Web. 2 May 2008. <http://www.futurepundit.com/archives/000940.html>.

Shen, Ching. *Rarefied Gas Dynamics*. New York: Springer, 2005. Print.

Shukla, P. K., and A. A. Mamun. *Introduction to Dusty Plasma Physics*. London: CRC Press, 2001. Print.

# FEASIBILITY STUDY OF HIGH ALTITUDE ATMOSPHERIC LAUNCHERS TO ORBIT

A Thesis

Presented to

The Faculty of the Department of Mechanical & Aerospace Engineering

San José State University

In Partial Fulfillment

of the Requirements for the Degree

Master of Science

by

Anna Rapo

December 2008

SAN JOSÉ STATE UNIVERSITY

The Undersigned Thesis Committee Approves the Thesis Titled

FEASIBILITY STUDY OF HIGH ALTITUDE
ATMOSPHERIC LAUNCHERS TO ORBIT

by
Anna Rapo

APPROVED FOR THE DEPARTMENT OF
MECHANICAL & AEROSPACE ENGINEERING

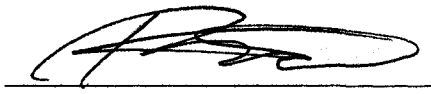

11/10/08

Dr. Periklis Papadopoulos, Department of Mechanical & Aerospace Engineering Date

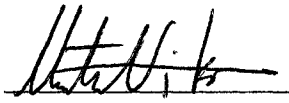

11-6-08

Dr. Nikos J. Mourtos, Department of Mechanical & Aerospace Engineering Date

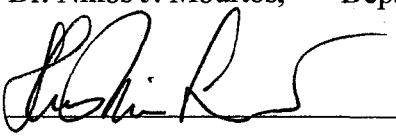

11-9-08

Dr. Sean Swei, National Aeronautics and Space Administration Date

APPROVED FOR THE UNIVERSITY

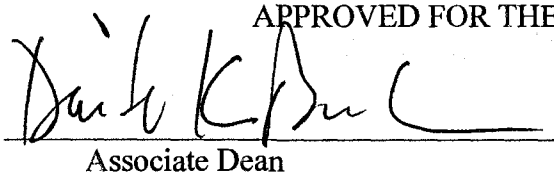

1/2/09

Associate Dean Date

ABSTRACT

FEASIBILITY STUDY OF HIGH ALTITUDE
ATMOSPHERIC LAUNCHERS TO ORBIT

by Anna Rapo

This thesis addresses the topic of launching an aerospace vehicle to orbit from a high altitude. The current transportation system from Earth to space has been deemed by many to be expensive, unreliable, and an unnecessarily dangerous means of travel to space. It is suggested in this proposal to examine a different type of launch from a high altitude to an orbit in space. By lifting the vehicle to a high altitude within Earth's atmosphere using a high-altitude balloon followed by the activation of the vehicle's propulsion system, a potentially cheaper and safer, though obviously longer journey, could be achieved to space.

ACKNOWLEDGEMENTS

To my mom and sister for being patient throughout both of my degrees, and taking me out running to freshen up those precious grey cells.

To my brothers whose support I felt even from thousands of miles away.

To my husband, I could not have accomplished all this without your love, and encouragement throughout the hard parts.

To my advisors for their wisdom and knowledge and to whom this work is largely due.

TABLE OF CONTENTS

LIST OF FIGURES

***Case 6: $h_0$ = 40 km, T/W = 10.19***

LIST OF TABLES

# NOMENCLATURE

| | |
|---|---|
| a | speed of sound |
| $\alpha$ | angle of attack |
| A | surface area of plate |
| $\beta$ | angle between velocity vector $\vec{V}$ and unit vector $\hat{\varphi}$ |
| Cl | lift coefficient |
| Cd | drag coefficient |
| D | drag force |
| $\vec{F}_c$ | centrifugal force |
| $F_{\parallel}$ | force acting in parallel to plate |
| $F_{\perp}$ | force acting perpendicularly to plate |
| $\gamma$ | adiabatic index |
| g | gravitational acceleration |
| $h_0$ | initial launch altitude |
| h | altitude |
| k | Boltzmann's constant |

| | |
|---|---|
| L | lift force |
| M | vehicle mass |
| Ma | Mach number |
| m | particle mass |
| n | number of particles |
| dp | momentum |
| P | pressure |
| $P_{acc}$ | coefficient of accommodation |
| dQ | energy |
| $\Phi_T$ | thrust angle |
| $d\Phi$ | incident particle flux |
| $\hat{\varphi}$ | unit vector along plane around the Earth |
| $\hat{r}$ | unit vector along the altitude plane |
| $R_E$ | radius of the Earth |
| $\rho$ | density of air |
| $\rho_a$ | density at altitude $h$ |

| | |
|---|---|
| $\rho_m$ | average mass density of vehicle |
| $\sigma$ | Stephan-Boltzmann's constant |
| $\theta_i$ | incident angle from normal perpendicular to surface |
| T | thrust force |
| u | velocity of particle |
| $\overline{v_>}$ | mean velocity of particles |
| W | weight of vehicle |

## Introduction

Expensive and risky, the current rocket transportation system from Earth to space is not favored by everyone. Based on technology from the 1970's, the expense of a trip to space remains in the hundreds of millions of dollars. As mentioned by Randall Parker in his article on FuturePundit.com, with a safety record that is still worse than aircraft travel when it was in its thirties, the current space travel technology is in dire need of a new direction for the sake of passenger safety, as well as assurance that expensive payload onboard gets delivered as scheduled safely to their destinations (Parker, 2008).

The research in this thesis examines a different type of launch during which a vehicle takes off from a high altitude balloon within Earth's atmosphere. Though this elongates the travel time, it may possibly reduce the dangers associated with the current rocket transportation system.

**Objective**

The objective of this thesis is to perform a feasibility study on the possibility of launching a vehicle from an atmospheric high altitude to an orbit in space.

This thesis reviews the forces acting on a body as it travels through the atmosphere's continuum region, while also considering atmospheric conditions at near space altitudes. The code developed recreates these launch conditions while providing information on the forces acting on the body. It also provides the position and velocity where the vehicle travels at given certain initials conditions. Finally, it presents a summary of the results, and their reliability.

## Background

According to HobbySpace.com, the highest elevation an unmanned research balloon has flown is nearly 52 km. This concept of high-altitude balloons carrying rockets has been around since the 1940's, affectionately nicknamed 'rockoons'. Unfortunately, due to the unstable nature of balloons, much research still needs to be done in stabilizing such a platform for a spacecraft to launch from (HobbySpace).

As mentioned before, the spacecraft in this thesis will be launched from an altitude and experience near space atmospheric conditions. The following two sub-sections will discuss the resulting equations of motion.

*Launch Trajectory Model*

The basic trajectory code model describes a flat plate traveling along a plane around the Earth as shown figure 1 (left diagram).

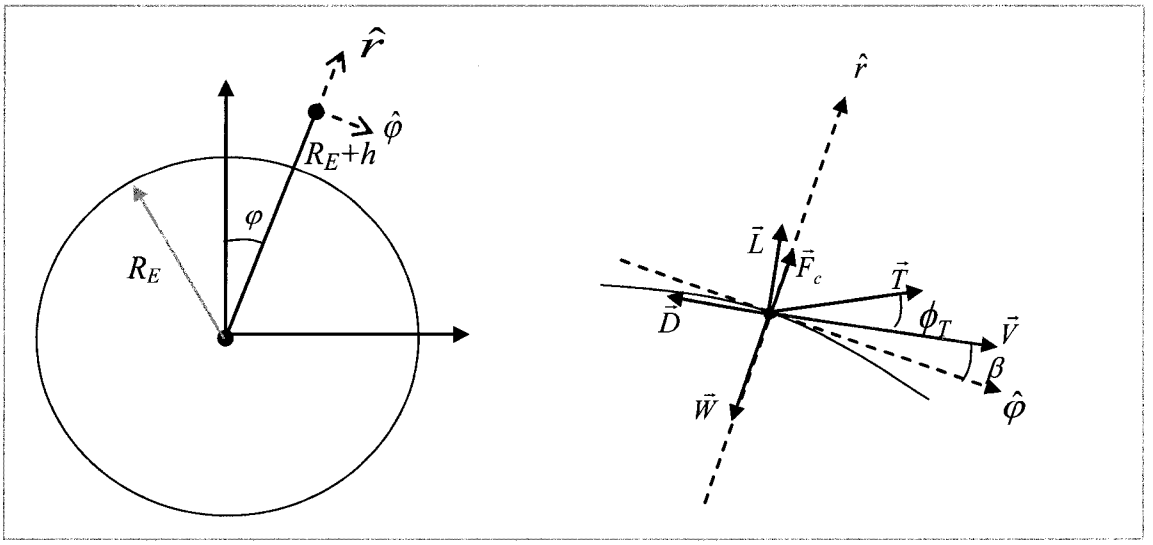

Figure 1. Representation of forces acting on vehicle.

Radius $r$ and angle $\varphi$ represent the vehicle's position in a polar coordinate system. Using unit vectors $\hat{\varphi}$ and $\hat{r}$ associated with this coordinate system, $V_\varphi$ and $V_r$ describe the velocity along those two vectors. The position of the vehicle can then be related to the velocities as follows:

$$r\frac{d\varphi}{dt} = V_\varphi \quad \text{and} \quad \frac{dh}{dt} = V_r \tag{1}$$

Note that $h$ represents the altitude.

The velocity vector is at an angle $\beta$ with $\hat{\varphi}$ and can be represented as follows:

$$V_\varphi = V\cos\beta \quad \text{and} \quad V_r = V\sin\beta$$

The forces acting on the vehicle are as shown on the right diagram of figure 1. The vehicle's own weight ($\vec{W}$) and centrifugal force ($\vec{F}_c$) are directed along the $\hat{r}$ vector. The lift force ($\vec{L}$) is shown perpendicular and the drag force ($\vec{D}$) parallel to velocity $\vec{V}$. The thrust vector ($\vec{T}$) is at angle $\phi_T$ with velocity $\vec{V}$. So the equations of motion of the vehicle become (Anderson, *Introduction* 393):

$$\begin{aligned} M\frac{dV_\varphi}{dt} &= T\cos(\phi_T+\beta) - D\cos\beta - L\sin\beta \\ M\frac{dV_r}{dt} &= T\sin(\phi_T+\beta) + L\cos\beta - D\sin\beta + M\frac{V_\varphi^2}{r} - Mg \end{aligned} \tag{2}$$

Within the position coordinate system, another coordinate system must be defined. Consider a flat plate at angle of attack $\alpha$. Unit vectors $\parallel$ and $\perp$ are parallel and perpendicular to the plate respectively as shown in figure 2.

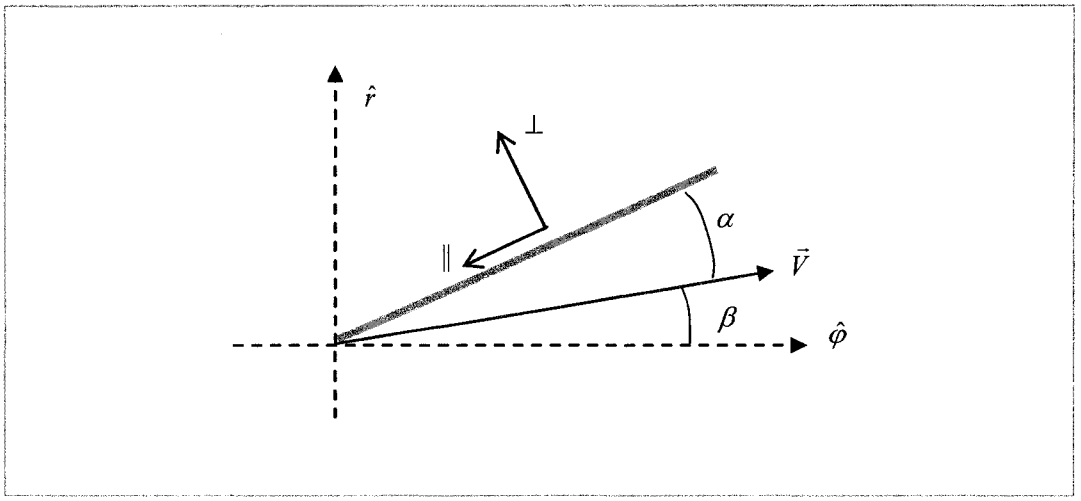

Figure 2. Representation of forces acting on plate while at angle α.

Along these unit vectors, forces $F_{\parallel}$ and $F_{\perp}$ are related to lift and drag forces as follows (257):

$$\begin{aligned} L &= F_{\perp}\cos\alpha - F_{\parallel}\sin\alpha \\ D &= F_{\perp}\sin\alpha + F_{\parallel}\cos\alpha \end{aligned} \tag{3}$$

Note that the drag force acts in the opposite direction from the velocity.

Substituting equations (3) into (2), the equations of motion are represented by:

$$\begin{aligned} M\frac{dV_{\varphi}}{dt} &= T\cos(\phi_T+\beta) - F_{\perp}\sin(\alpha+\beta) - F_{\parallel}\cos(\alpha+\beta) \\ M\frac{dV_{r}}{dt} &= T\sin(\phi_T+\beta) + F_{\perp}\cos(\alpha+\beta) - F_{\parallel}\sin(\alpha+\beta) + M\frac{V_{\varphi}^2}{r} - Mg \end{aligned} \tag{4}$$

By assuming certain initial conditions at time t = 0, the next velocity components and therefore angle $\beta$ can be calculated for the next time step using the equations (4). The following position of the vehicle is recalculated using equations (1). The altitude

during one time step helps compute the air density and aerodynamic forces acting on the vehicle for the following step.

Though the thrust angle is initially assumed, there are 3 thrust angles cases that must be considered. First case being that $\phi_T = 0$ and $\vec{T}$ is always along $\vec{V}$. The second scenario is where $\phi_T = \alpha$ and $\vec{T}$ is along the chord length. The final case is where $\phi_T = -\beta$ and $\vec{T}$ is always along $\hat{\varphi}$.

Since the aerodynamic forces are proportional to the vehicle's surface area ($A$), and dynamic pressure ($\rho V^2$), we divide both sides of equations (4) by the vehicle mass to get:

$$\begin{aligned} \frac{dV_\varphi}{dt} &= \frac{T}{W} g \cdot \cos(\phi_T + \beta) - \frac{F_\perp}{M} \sin(\alpha+\beta) - \frac{F_\parallel}{M} \cos(\alpha+\beta) \\ \frac{dV_r}{dt} &= \frac{T}{W} g \cdot \sin(\phi_T + \beta) + \frac{F_\perp}{M} \cos(\alpha+\beta) - \frac{F_\parallel}{M} \sin(\alpha+\beta) + \frac{V_\varphi^2}{r} - g \end{aligned} \tag{5}$$

*Trajectory Model in Near Space with Specular-Diffusive Interaction*

Near space is considered to lie between 20 - 100 km in altitude. It's a range of very low density. As this altitude is part of the trajectory presented in this thesis, the forces acting on the vehicle traveling across that altitude also need to be presented.

Consider the following scenario where a flux of incident particles reflects off a surface at an angle $\theta_i$ from the normal. The thermal spreading of these particles can be considered negligible, and angle $\alpha$ is the angle of attack from the surface. The unit area

$dA$ on the wall onto which the particles hit project an area $dA\cos\theta_i$ as shown in figure 3 (Shen 169). The flux of particles through this area can be represented as follows (Loeb 42-43):

$$d\Phi = n \cdot u \cdot dA\cos\theta_i \tag{6}$$

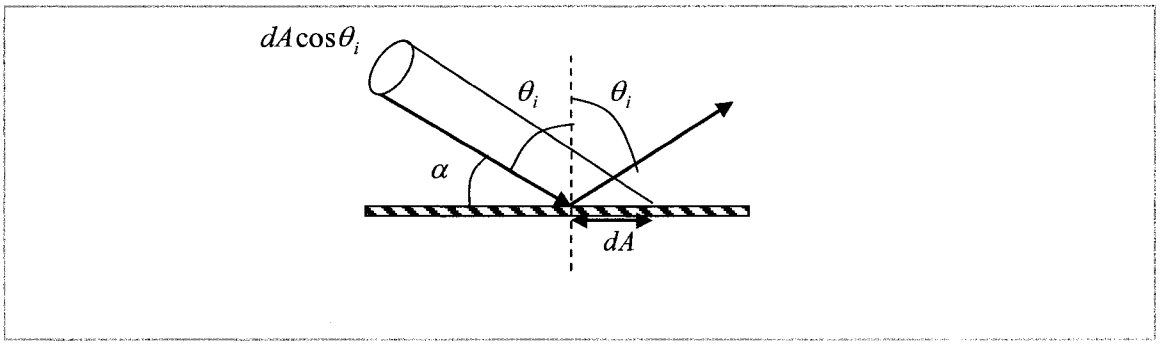


Figure 3. Reflection of incident particles on surface.

For the case of specular reflection (figure 4), the particle bounces perfectly from the surface at the same angle it arrived at while fully conserving its energy (Shen 132). The momentum and energy transferred to the surface are then respectively (Loeb 18-19):

$$\begin{aligned} dp_{\perp} &= 2mu\cos\theta_i \\ dp_{\parallel} &\equiv 0 \\ dQ &\equiv 0 \end{aligned} \tag{7}$$

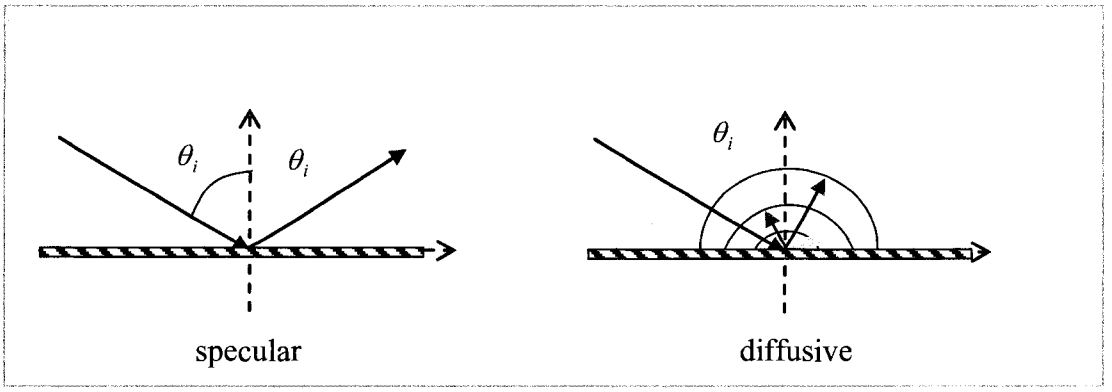


Figure 4. Specular and diffuse reflection.

During diffusive reflection, the particles reflect according to Maxwellian distribution. This occurs at material temperature $T_m$ in the half-space of $0<\theta<\pi/2$. The momentum absorbed can be represented by (Shen 132, 162):

$$\begin{aligned} dp_{\perp} &= m(u\cos\theta_i + \overline{v_>}) \\ dp_{\parallel} &= mu\sin\theta_i \end{aligned} \tag{8}$$

where the mean velocity, $\overline{v_>}$, (equation A.3b, Appendix A) at the material temperature $T_m$:

$$\overline{v_>} = \left(\frac{kT_m}{2\pi m}\right)^{\frac{1}{2}} \tag{9}$$

By multiplying the particle flux with the momentum equations, the tangential and normal forces projected on the surface are found and shown in table 1.

Table 1. Normal and tangential equations for specular and diffusive reflection.

| Specular | Diffuse |
|---|---|
| $dF_{\perp} = dA\cdot 2\rho u^2\cos^2\theta_i$ <br> $dF_{\parallel} \equiv 0$ | $dF_{\perp} = dA\cdot\rho u\cos\theta_i\left[u\cos\theta_i + \overline{v}_>\right]$ <br> $dF_{\parallel} = dA\cdot\rho u^2\cos\theta_i\sin\theta_i$ |

(10)

Translating them onto a Cartesian coordinate system, the equations (10) become:

$$\begin{aligned} dF_x &= -dF_{\perp}\sin\alpha - dF_{\parallel}\cos\alpha \\ dF_y &= +dF_{\perp}\cos\alpha - dF_{\parallel}\sin\alpha \end{aligned} \quad \text{since} \quad \begin{aligned} \sin\alpha &= \cos\theta_i \\ \cos\alpha &= \sin\theta_i \end{aligned} \tag{11}$$

The relationship between the unit vectors $\parallel$ and $\perp$, and the x- and y-coordinate system is shown in figure 5. The forces *per unit area* are then shown in table 2.

Table 2. Forces per unit area according to a Cartesian coordinate system.

| Specular | Diffuse |
|---|---|
| $df_x = -2\rho u^2 \sin^3\alpha$<br>$df_y = +2\rho u^2 \sin^2\alpha\cos\alpha$ | $df_x = -\rho u^2 \sin\alpha - \rho u \sin^2\alpha \cdot \overline{v_>}$<br>$df_y = +\rho u \sin\alpha\cos\alpha \cdot \overline{v_>}$ |

(12)

The coefficient of accommodation $P_{acc}$ represents the likelihood the particles will behave more according to a perfect diffuse model than a perfect reflective model (Shukla and Mamun 80). A $P_{acc}$ value of unity would be considered a perfect diffusive reflection. For simplicity, we assumed this probability to be a constant, though it usually depends on surface conditions, particle energy, incident angle, and other factors. For our case, $P_{acc}$ was assumed to be 0.1 due to the high temperatures the plate was expected to experience, as well as the cleanliness and smoothness of the plate's surface assumed (Loeb 336).

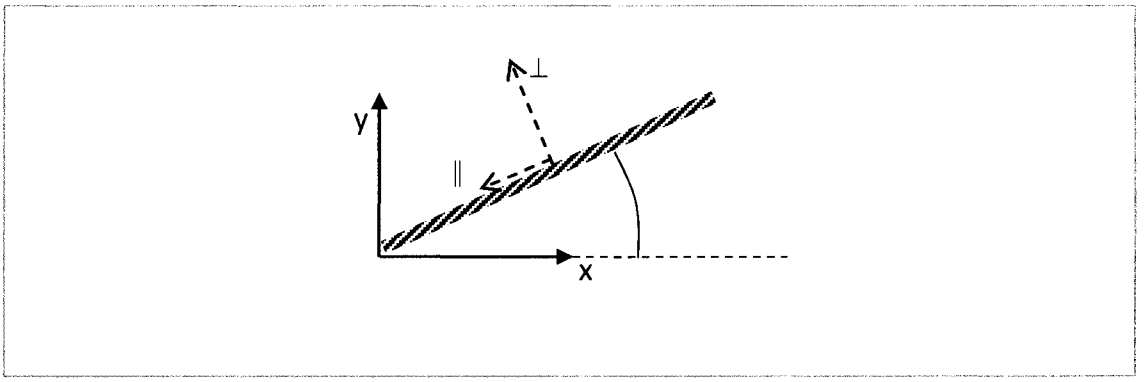


Figure 5. Change of coordinate system.

Each particle transfers energy onto the wall in the amount of $u^2/2$. Meanwhile, the energy lost by the wall when reflecting a particle is the average energy shown by equation (A-4b) in Appendix A. Finally, the wall was assumed to behave like a black body. The resulting equations for the forces and energy transferred per unit area are:

$$
\begin{aligned}
df_x &= -\rho u^2 \left[ 2(1-P_{acc}) \sin^3\alpha + P_{acc} \sin\alpha + P_{acc} \sin^2\alpha \frac{\overline{v_>}}{u} \right] \\
df_y &= +\rho u^2 \left[ 2(1-P_{acc}) \sin^2\alpha \cos\alpha + P_{acc} \sin\alpha \cos\alpha \frac{\overline{v_>}}{u} \right] \\
dq &= \rho u \sin\alpha \frac{u^2}{2} - \rho u P_{acc} \sin\alpha \cdot \left( \frac{3kT_m}{4m} \right) - \sigma T_m^4
\end{aligned}
\tag{13}
$$

By including thrust, gravity, and centrifugal force that contributed to the vehicle's dynamics, the equations become:

$$
\begin{aligned}
M\frac{du}{dt} &= T_x - A\rho u^2 \left[ 2(1-P_{acc}) \sin^3\alpha + P_{acc} \sin\alpha + P_{acc} \sin^2\alpha \frac{\overline{v_>}}{u} \right] \\
M\frac{dv}{dt} &= T_y + M\frac{u^2}{R_E + h} - Mg + A\rho u^2 \left[ 2(1-P_{acc}) \sin^2\alpha \cos\alpha + P_{acc} \sin\alpha \cos\alpha \frac{\overline{v_>}}{u} \right]
\end{aligned}
\tag{14}
$$

The forces can be normalized by the weight, and using an average area mass density $\rho_m$ for the vehicle:

$$
\begin{aligned}
\frac{du}{dt} &= \frac{T_x}{W} g - \frac{\rho_a}{\rho_m} u^2 \left[ 2(1-P_{acc}) \sin^3\alpha + P_{acc} \sin\alpha + P_{acc} \sin^2\alpha \frac{\overline{v_>}}{u} \right] \\
\frac{dv}{dt} &= \frac{T_y}{W} g + \frac{u^2}{R+h} - g + \frac{\rho_a}{\rho_m} u^2 \left[ 2(1-P_{acc}) \sin^2\alpha \cos\alpha + P_{acc} \sin\alpha \cos\alpha \frac{\overline{v_>}}{u} \right]
\end{aligned}
\tag{15}
$$

Recall that $W = Mg$, $\rho_a(h) = \rho_o \exp(-h/h_o)$, and $\frac{dh}{dt} = v$.

In addition to the previous equations, the code calculates the Mach number at every point of the trajectory. The following equation was used to find the speed of sound (Anderson, *Introduction* 159):

$$
a = \sqrt{\gamma P / \rho} \tag{16}
$$

where we used the adiabatic index, $\gamma = 1.4$. P represents pressure, and $\rho$ is the density of air. Therefore the Mach number can be found through (160):

$$Ma = V_{FREESTREAM} / a \tag{17}$$

After results were produced by the code, the following equations were used to calculate the lift and drag coefficients with A representing the plate's surface area:

$$C_L = \frac{L}{0.5(\rho_{AIR})V_{FREESTREAM}{}^2 A}$$
$$C_D = \frac{D}{0.5(\rho_{AIR})V_{FREESTREAM}{}^2 A} \tag{18}$$

For subsonic compressible flow ($0.3 < Ma < 1$), the lift coefficient becomes (Anderson, *Aerodynamics* 691-693):

$$C_L = \frac{2\pi\alpha}{\sqrt{1-Ma^2}}$$

For supersonic flow between Mach ($1 < Ma < 5$), the following equations were used:

$$C_L = \frac{4\alpha}{\sqrt{Ma^2-1}}$$
$$C_D = \frac{4\alpha^2}{\sqrt{Ma^2-1}}$$

For hypersonic flow ($Ma > 5$), the equations used were as follows:

$$C_L = 2\sin^2\alpha(\cos\alpha)$$

$$C_D = 2\sin^3\alpha$$

## Methodology

The launch conditions needed to be simulated in varying high altitude environments. This was achieved by using the MatLab software that is now so commonly used in the aerospace and many other industries.

The code developed (Appendix B) is based on the previously mentioned model that calculates the forces affecting a flat plate as it gains altitude. It takes into consideration air density changes with altitude, angles of attack, weight, initial altitudes of launch, and initial thrust. The equations used in this code also take into consideration spectral and diffusive reflection for near space conditions. By adding a few computation boundaries such as achieving orbital velocity (8 km/s), space orbit (150 km), or if the altitude drops to less than zero, the code breaks displaying a message whether the launch was successful or not.

Two altitudes serve as the initial launch locations, 20 and 40 km. These are altitudes through which current high-altitude balloons are able to achieve. Because the code supplies information on altitude, distance, density, velocity, forces and Mach numbers at every point of the launch trajectory, a parametric study was possible between all the variables.

The parametric study performed included trade studies between the different variables, lift and drag coefficients, altitude, and vehicle velocities in the x- and y-direction at varying angles of attack, as to analyze which scenario resulted in the best

launch. The parametric study also helped determine whether the code was giving valid results.

**Results**

The following pages show the results achieved with the code. Table 3 includes the scenarios considered. Microsoft Excel was used to graph all the cases.

Table 3. Cases considered.

| Case No. | Thrust to Weight Ratio (T/W) | Altitude ($h_0$), km | Angle of attack ($\alpha$), degrees |
|---|---|---|---|
| 1 | 1.5 | 20 | 5°, 10° |
| 2 | 5.1 | 20 | 1°, 5°, 10°, 15° |
| 3 | 10.19 | 20 | 1°, 5°, 10°, 15° |
| 4 | 1.5 | 40 | 5°, 10°, 15° |
| 5 | 5.1 | 40 | 1°, 5°, 10°, 15° |
| 6 | 10.19 | 40 | 1°, 5°, 10°, 15° |

*Case 1: $h_0$ = 20 km, T/W = 1.53*

Figure 6 displays the trajectory of the flat plate at different angles of attack. Flights at angles of attack of 5° and 10° were considered to be the only successful flights. It can be observed that the higher the angle of attack, the earlier the velocity boundary (8 km/s) is achieved, and the code breaks.

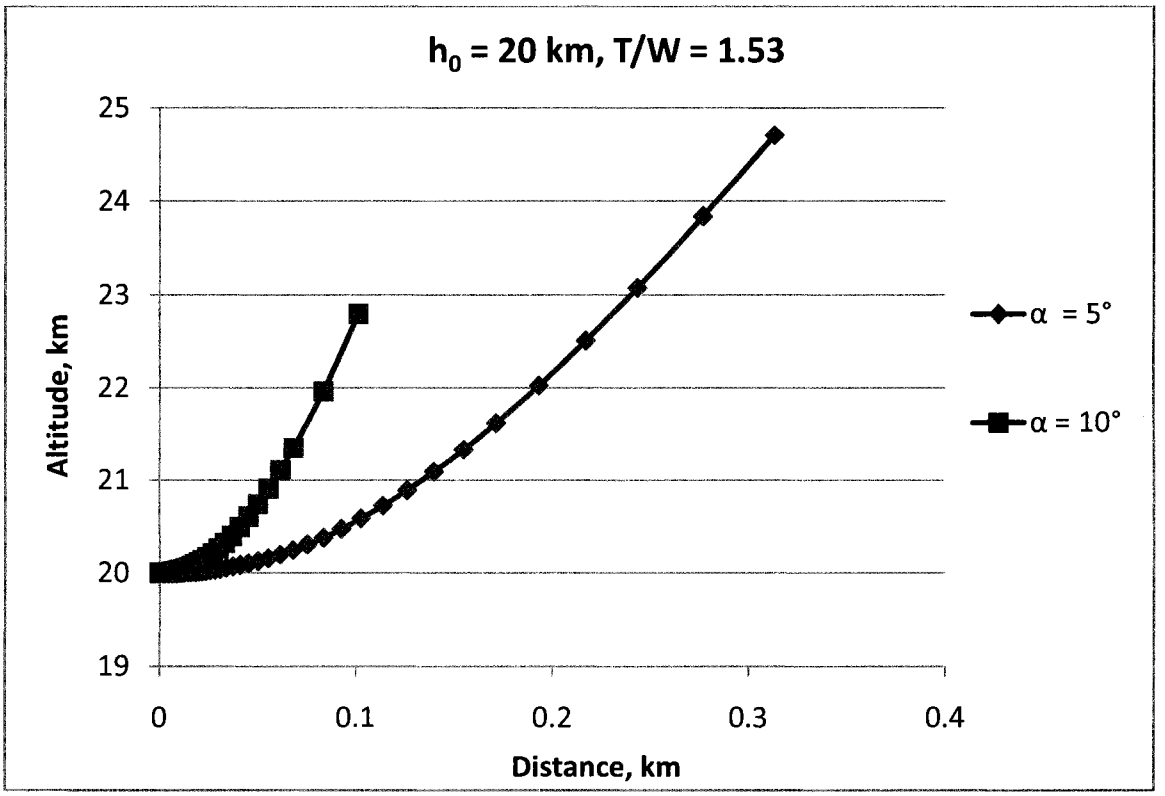


Figure 6. Distance versus altitude for $h_0$ = 20 km and T/W = 1.53.

Figure 7 shows that the lower the angle of attack, the higher the altitude required to achieve the velocity requirement.

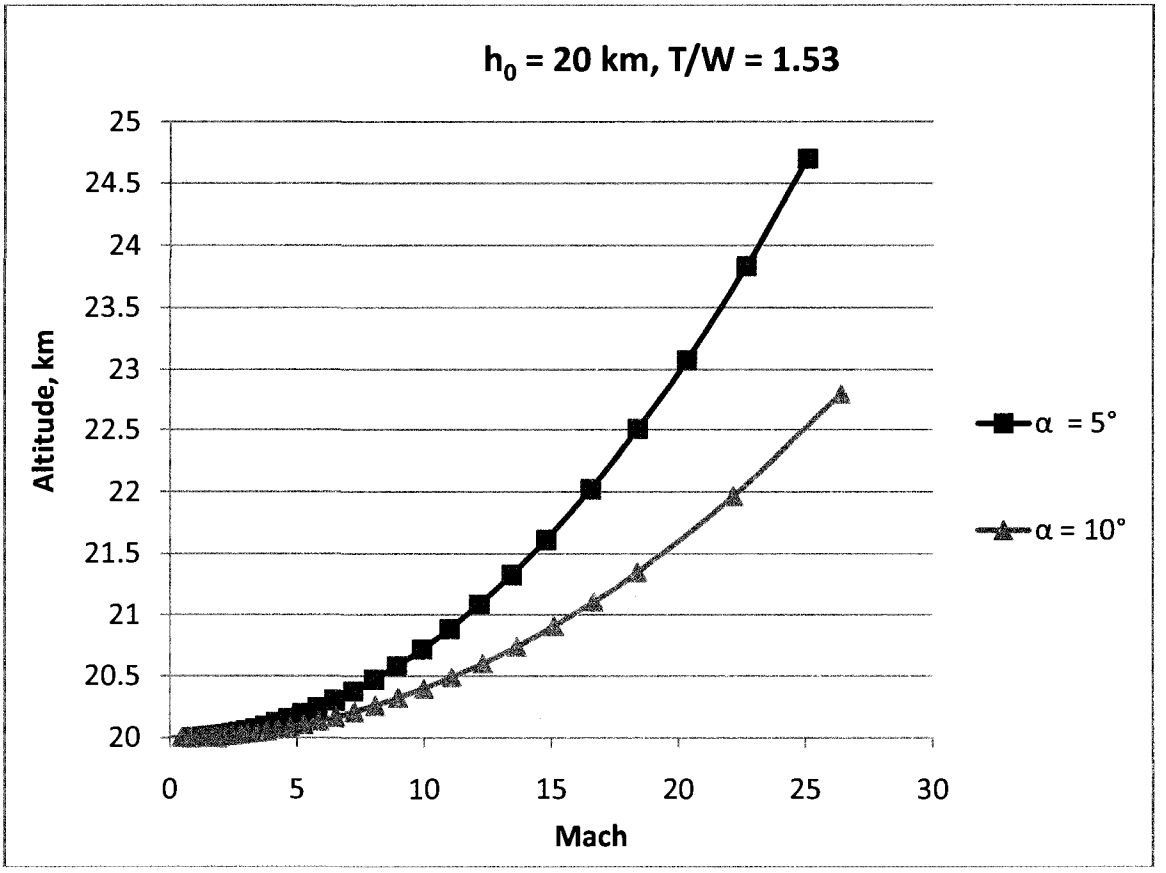


Figure 7. Mach number versus altitude.

Figure 8 focuses on the behavior of the drag and lift coefficients for Mach numbers 1 through 24. Examining the graph from right to left shows that the lift coefficient and drag coefficient being high upon takeoff with a linear decrease. An angle of attack of $\alpha = 5°$ results in a higher L/D ratio of approximately 11. At $\alpha = 10°$, its L/D ratio is 6. A higher attack angle will have more drag and therefore a lower Cl/Cd ratio, as shown in figure 8.

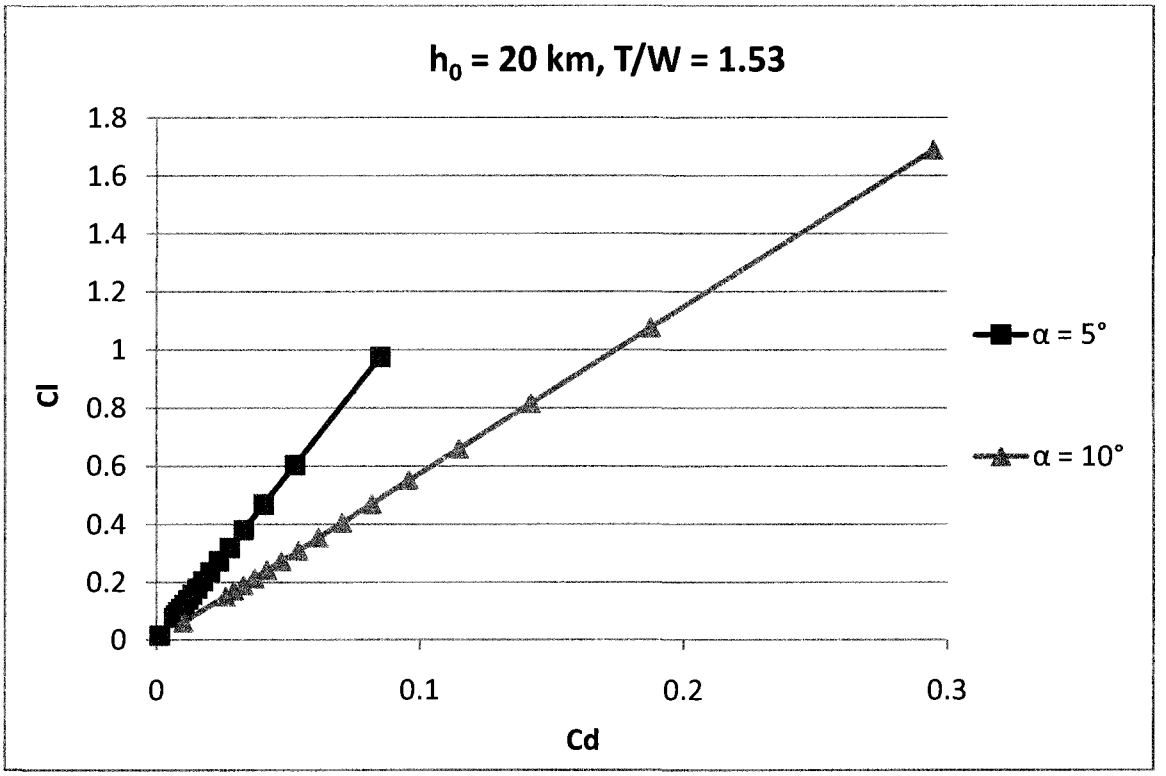


Figure 8. Drag coefficient versus lift coefficient for M = 1 through 24.

Figure 9 displays the lift coefficient with respect to Mach number upon takeoff to Mach 24. The lift coefficient increases to infinity from Mach 0 to 1. As the Mach number continues increasing to 25, the lift coefficient decreases. As displayed, the higher the attack angle, the higher the lift coefficient as the Mach number increases.

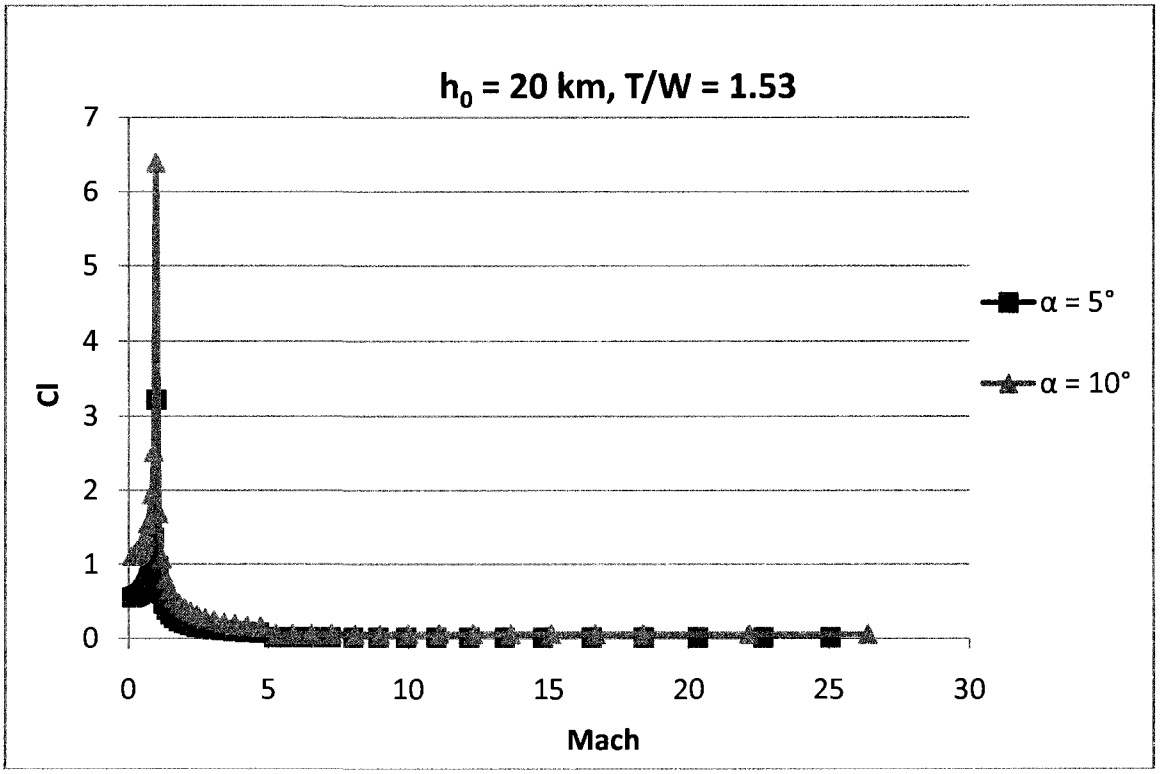

Figure 9. Mach number versus lift coefficient.

*Case 2: $h_0$ = 20 km, T/W = 5.1*

Figure 10 displays the trajectory of the flat plate at different angles of attack from an initial altitude of 20 km at T/W = 5.1. Figure 11 shows a close-up of the higher attack angles. As shown, the higher the attack angle, the lower the trajectory route it takes to achieve the velocity requirement of 8 km/s. When comparing to case 1 in figure 6, a higher T/W ratio also improves the trajectory distance in which the Mach 24 velocity requirement is achieved. The results for an attack angle of 1° were included as the launch was considered a successful run.

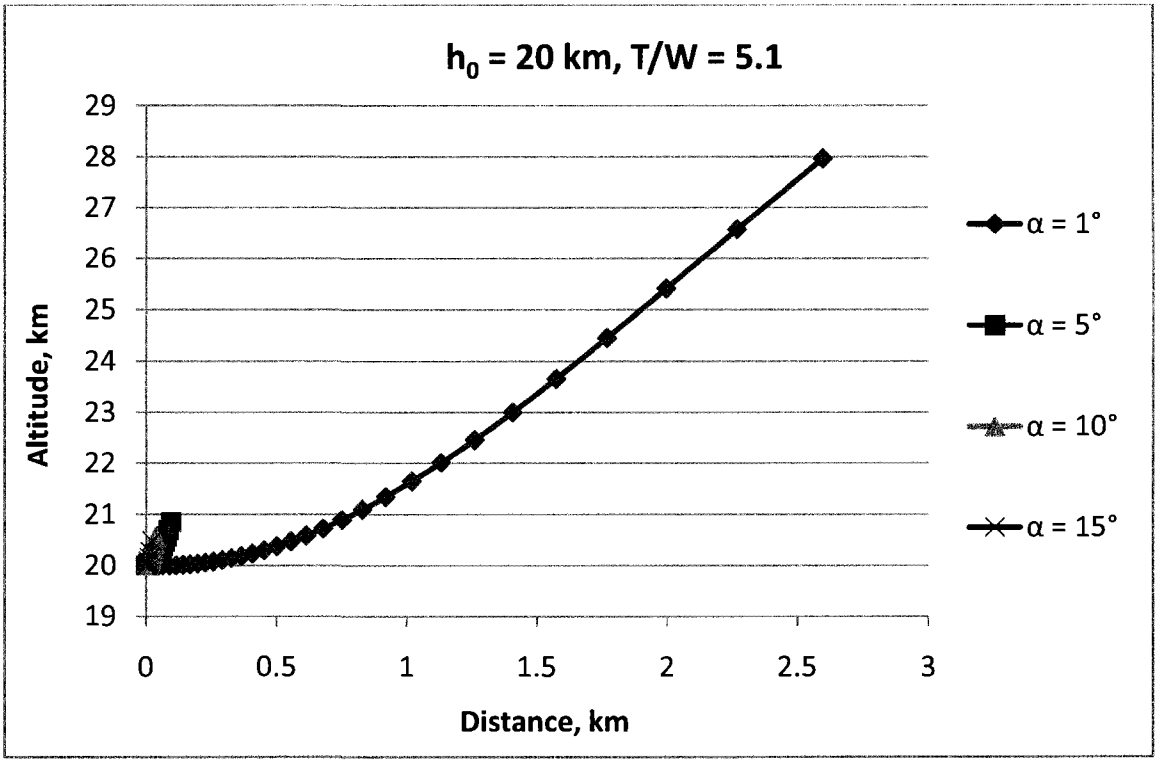


Figure 10. Distance versus altitude for $h_0$ = 20 km and T/W = 5.1.

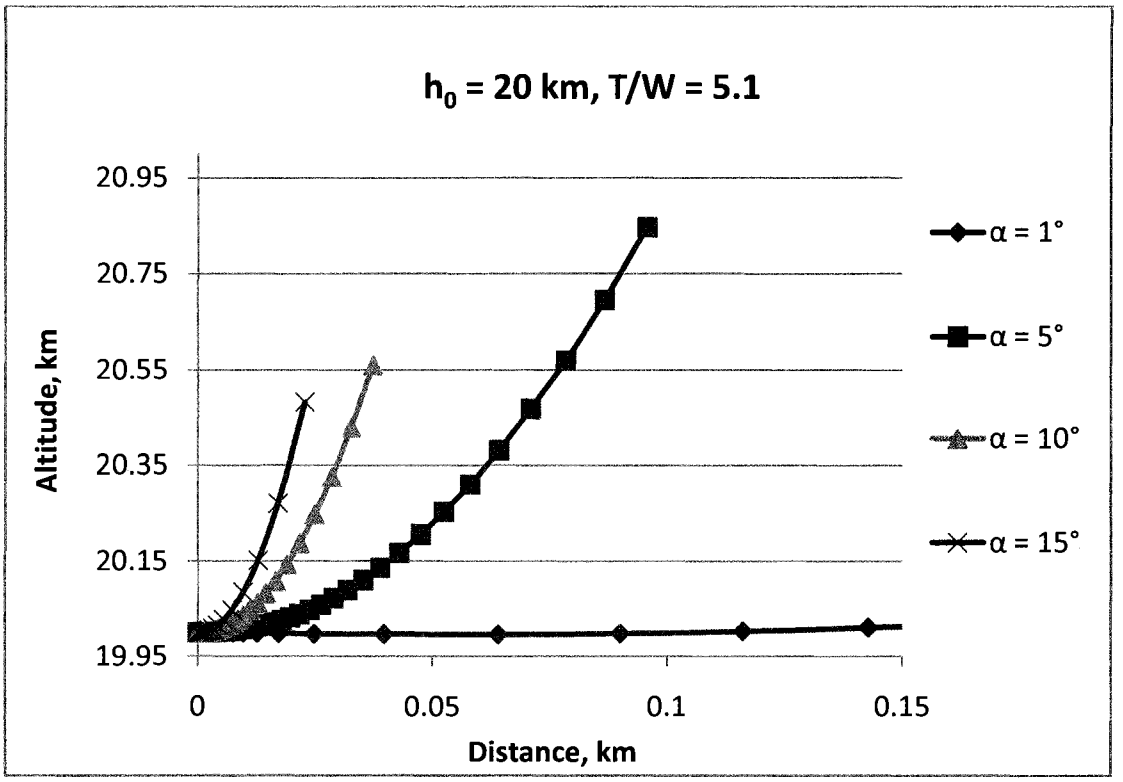

Figure 11. Close-up of altitude-distance curves for α = 5°, 10° and 15°.

Figure 12 demonstrates again the familiar trend of lower angles of attack requiring longer to achieve 8 km/s in velocity. Comparing with figure 7, the final altitude value is reduced with a higher thrust to weight ratio to achieve its final velocity.

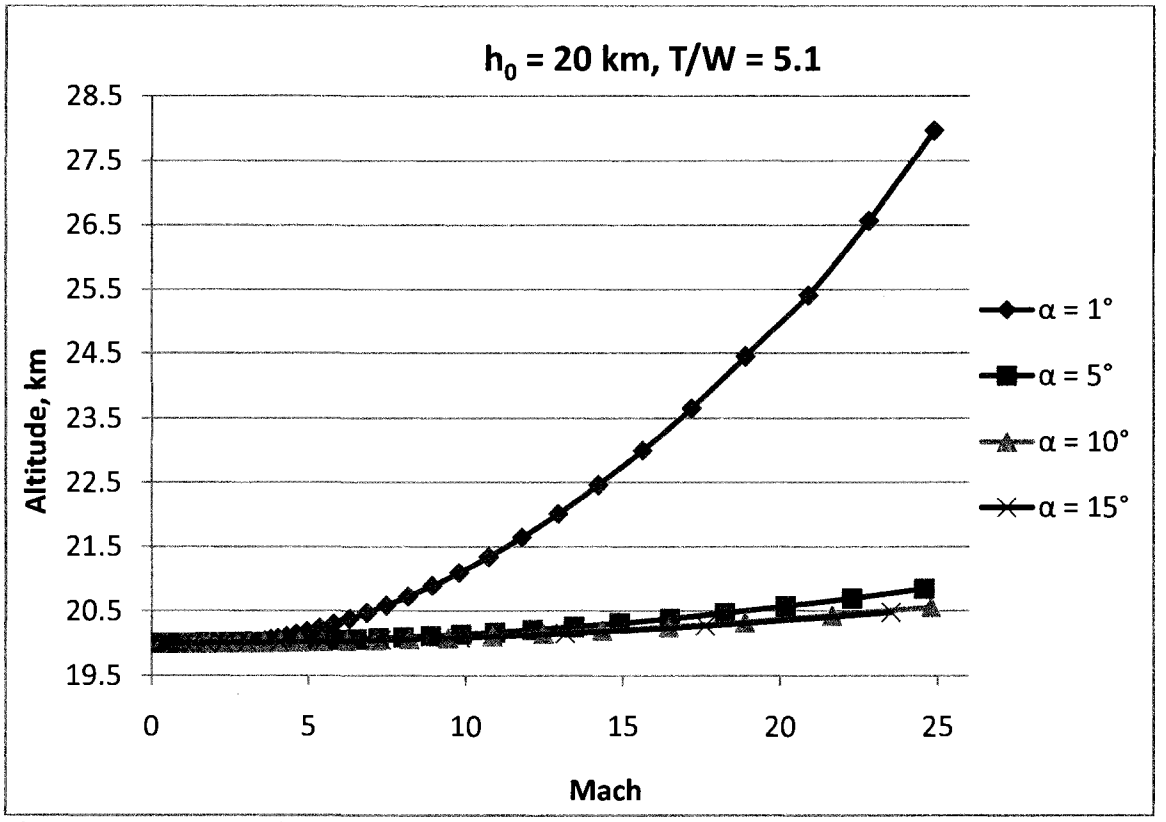

Figure 12. Mach number versus altitude.

When comparing to figure 8, figure 13 shows the same trend that the lift coefficient and drag coefficients decrease with Mach number. As the angles of attack are lower, the smaller the lift and drag coefficients but the higher Cl/Cd ratio. This graph only considers results beyond Mach 1.

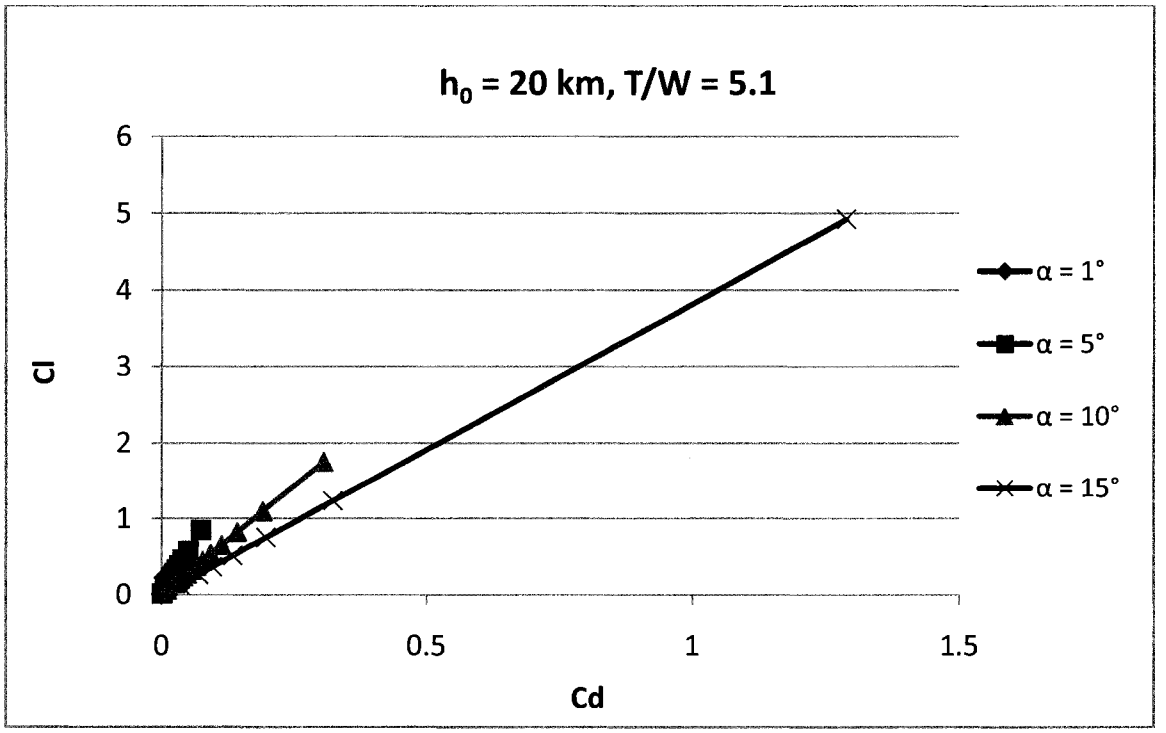

Figure 13. Drag coefficient versus lift coefficient for M = 1 through 24.

Figure 14 shows again the familiar pattern of the lift coefficient increasing from Mach 0 to Mach 1 and decreasing as the Mach number approaches a value of 25. Lower attack angles have lower lift coefficients than higher angles of attack.

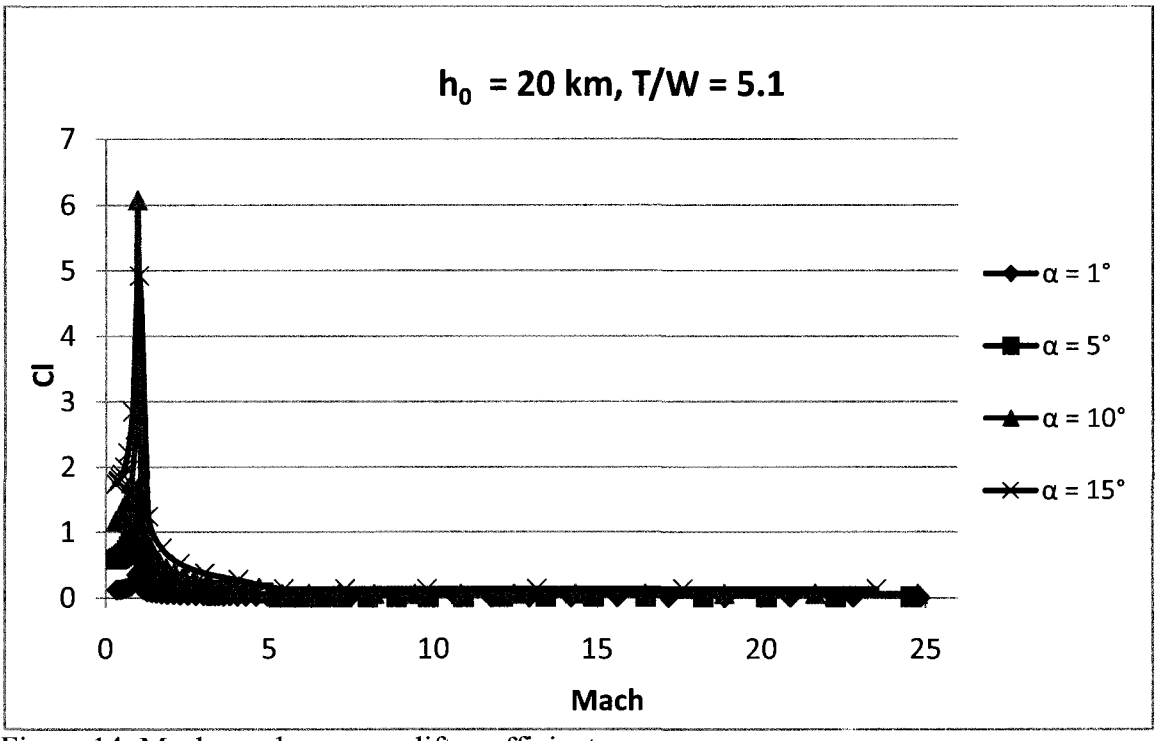

Figure 14. Mach number versus lift coefficient.

*Case 3: $h_0$ = 20 km, T/W = 10.19*

At T/W = 10.19 (figures 15 and 16), the velocity requirement is achieved at even shorter trajectory courses when compared to figures 6 and 10. When taking a closer look at higher angles of attack (figure 16), their results show a stable and predictable flight behavior.

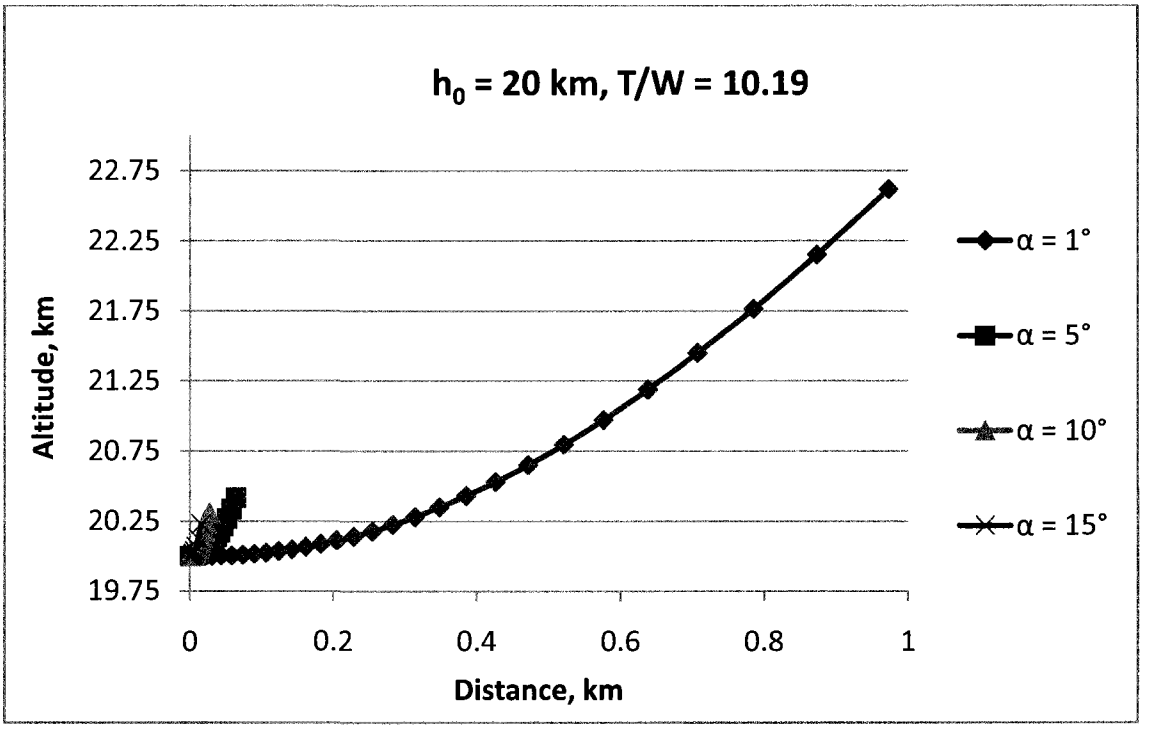


Figure 15. Distance versus altitude for $h_0$ = 20 km and T/W = 10.19.

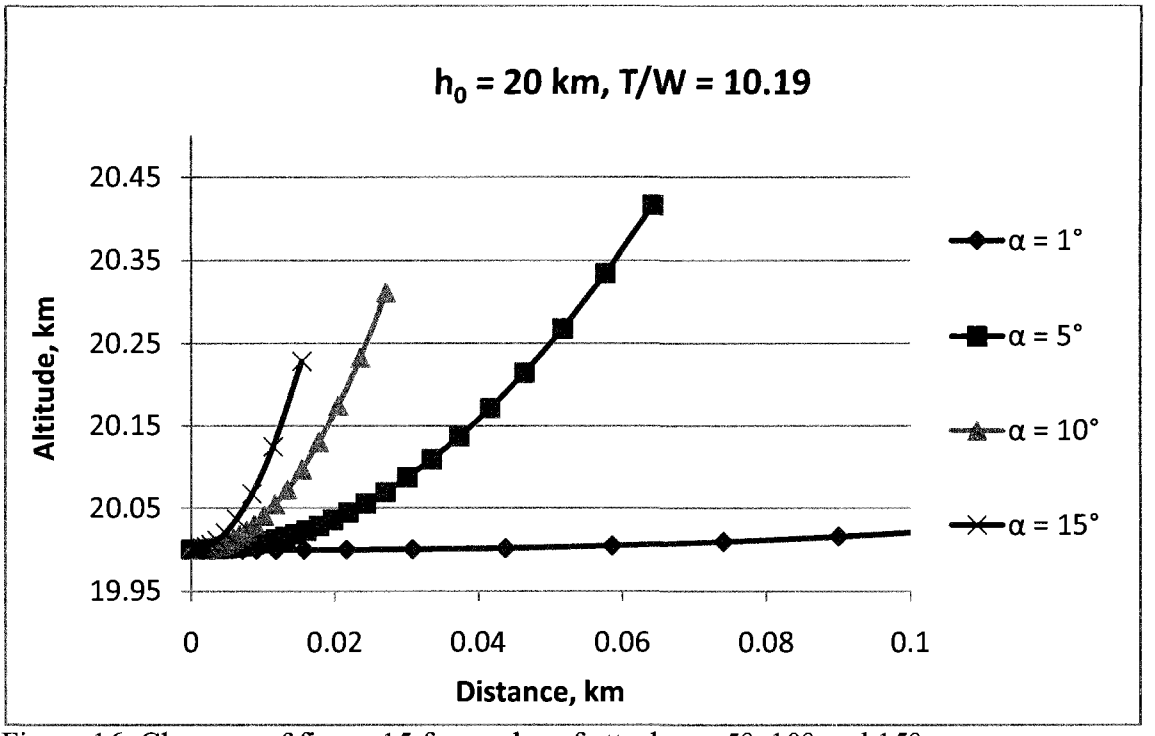

Figure 16. Close-up of figure 15 for angles of attack α = 5°, 10° and 15°.

Comparing figure 17 with figures 7 and 12, the final altitude value is reduced with a higher thrust to weight ratio though not by much for angles 5°, 10°, 15° and 20°. The only results with dramatic improvements in final altitude were for $\alpha = 1°$.

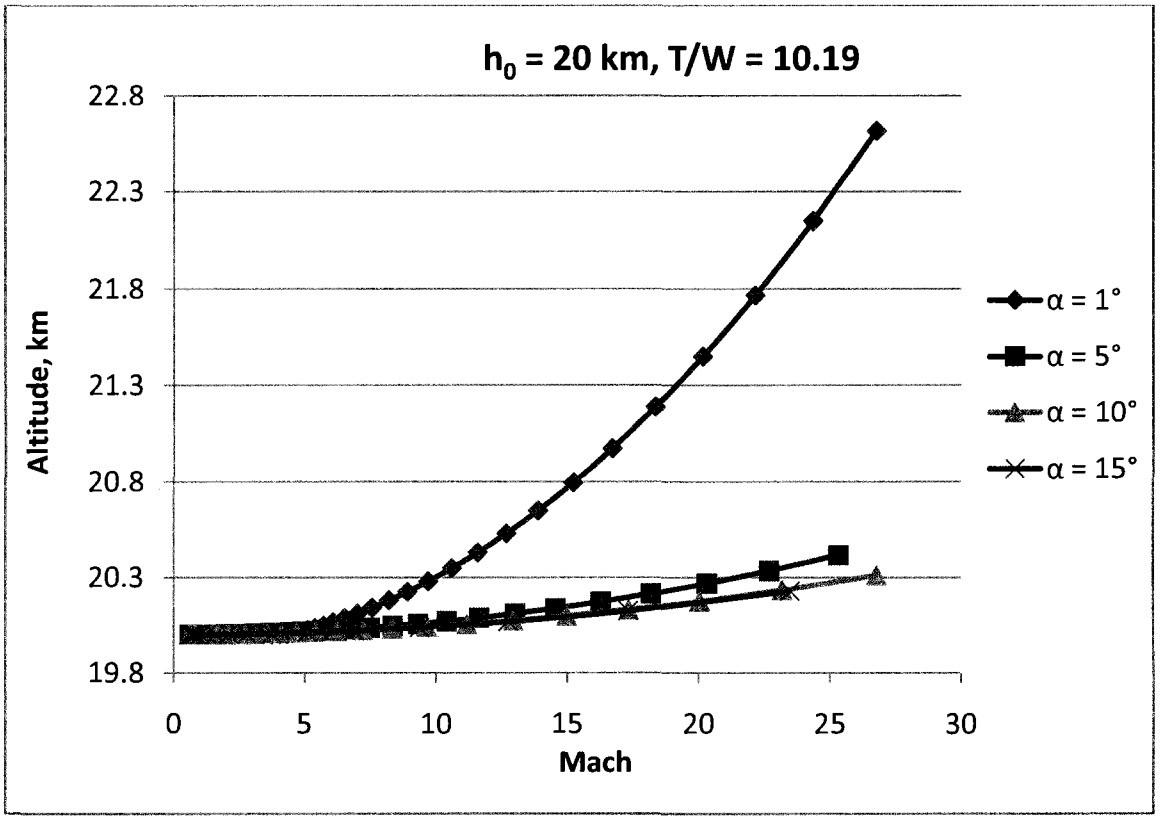

Figure 17. Mach number versus altitude.

When comparing figure 18 with figures 8 and 13, the same trend occurs where the higher the angle of attack the lower the lift coefficient to drag coefficient ratio. Figure 18 shows a close-up of the results for an attack angle of 1°.

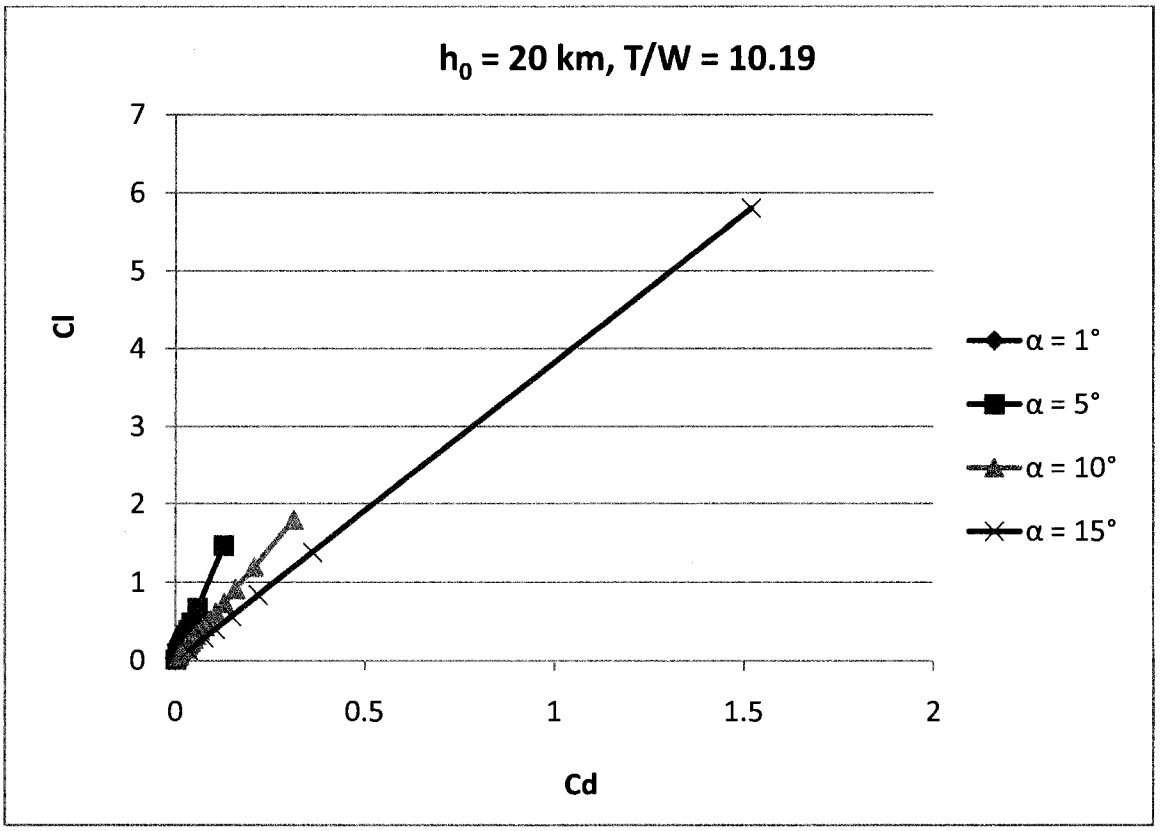

Figure 18. Drag coefficient versus lift coefficient for M = 1 through 24.

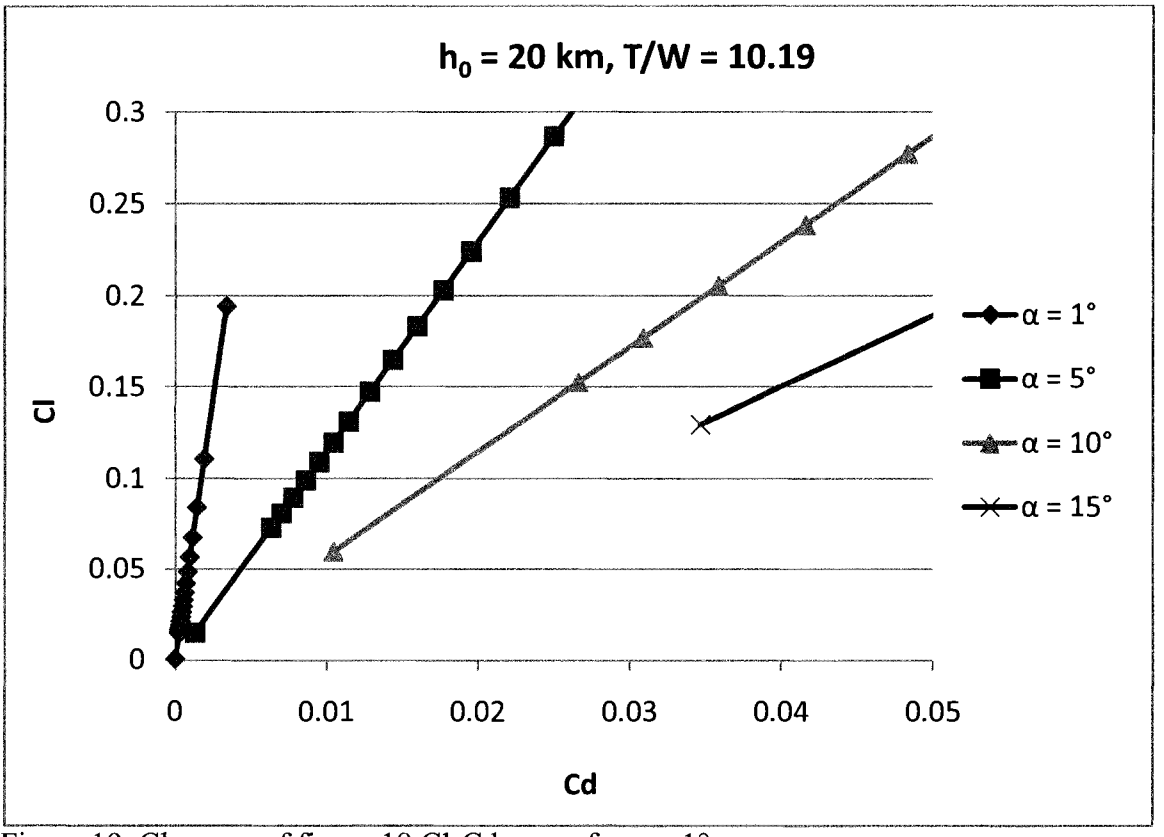

Figure 19. Close-up of figure 18 Cl-Cd curve for α = 1°.

Figure 20 demonstrates a higher lift coefficient for a higher attack angle. At Mach 1, the lift coefficient increases to infinity though here they are shown to have a finite value. This is due to the computation occurring at different proximities of Mach 1 resulting in a high Cl. The Cl values should be treated to be infinity at Mach 1 for all cases of this study.

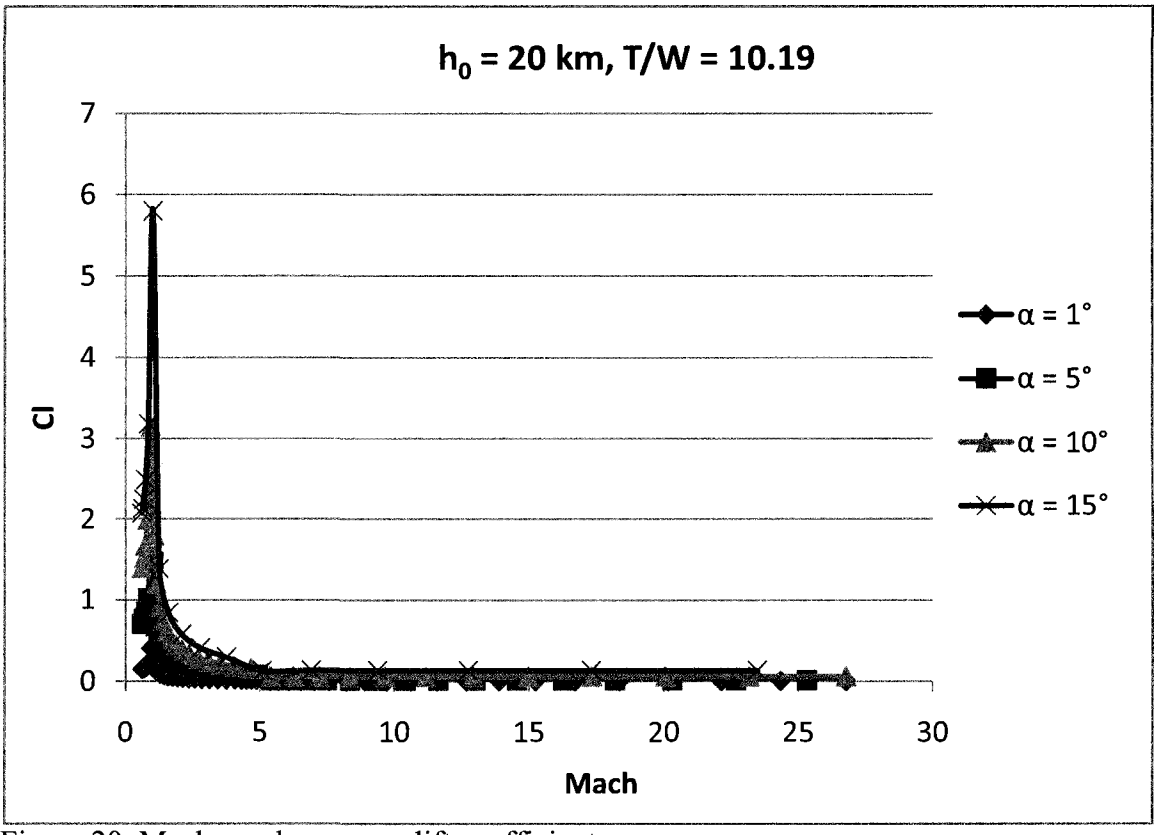

Figure 20. Mach number versus lift coefficient.

*Case 4: $h_0$ = 40 km, T/W = 1.53*

Figure 21 shows the trajectories for $h_0$ = 40 km. The results at an angle of attack of 1° were omitted due to an unsuccessful run. As shown here, successful launches occurred for all other angles of attack. The general trend was that at higher attack angles their velocity requirement was achieved at a smaller trajectory distance.

When comparing to the previous three cases, a higher altitude shows an advantage of launching at a wider range of angles successfully.

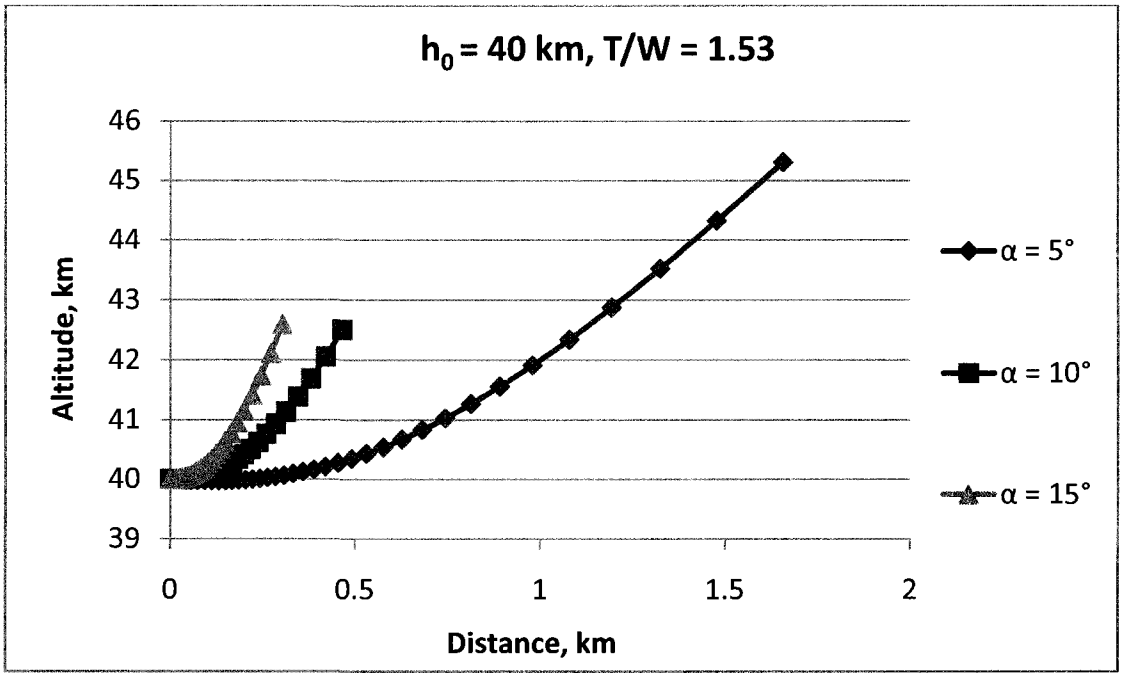

Figure 21. Distance versus altitude for $h_0$ = 40 km and T/W = 1.53.

Comparing figure 22 with figure 7 with the same thrust to weight ratio, it takes longer and a lower attack angle for the vehicle launching at a higher altitude to achieve its final velocity of 8 km/s.

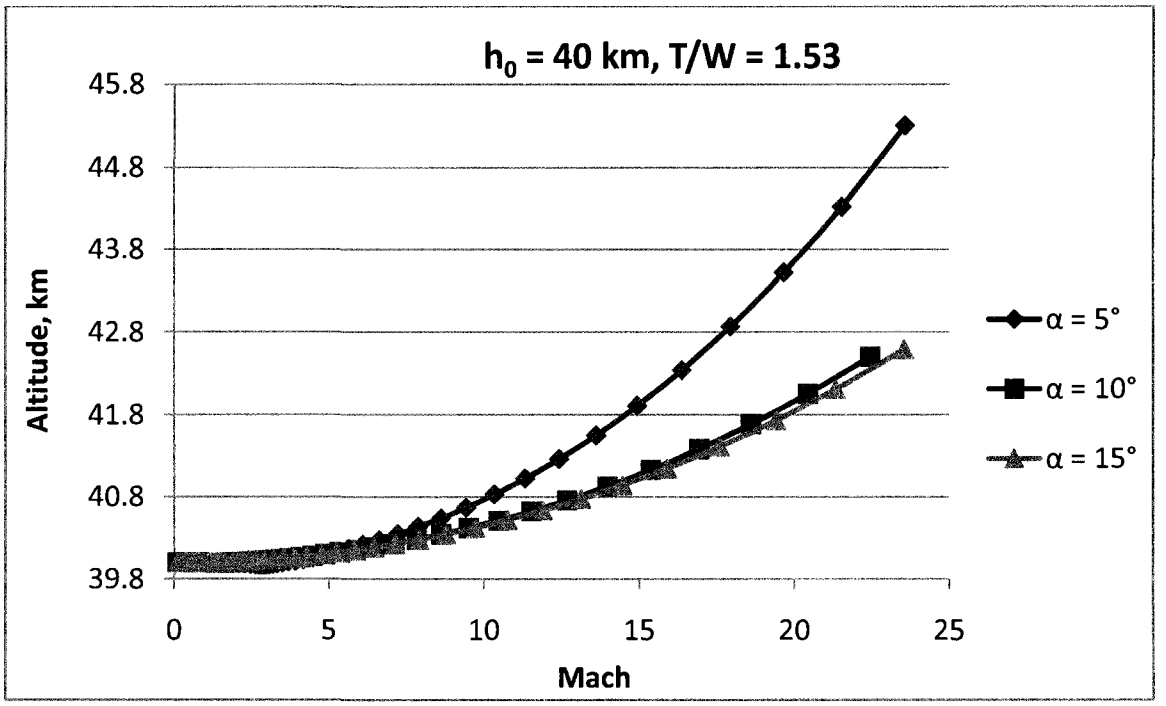

Figure 22. Mach number versus altitude.

Figure 23 shows the familiar trend of higher Cl/Cd ratios for lower angles of attack.

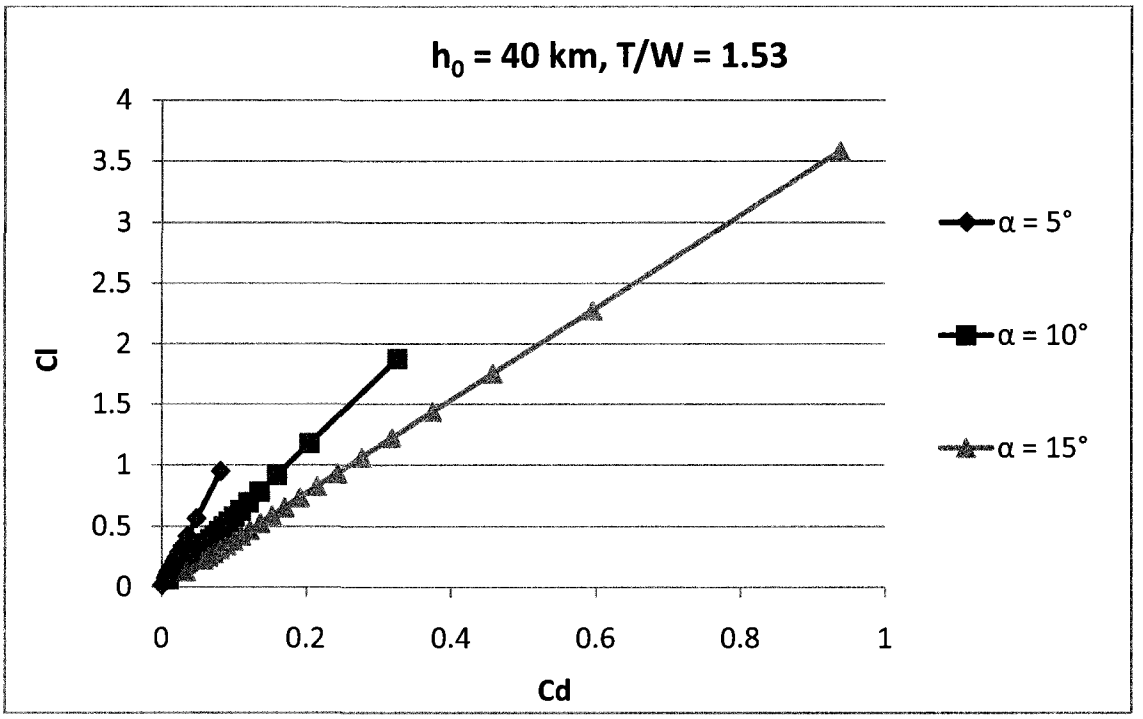

Figure 23. Drag coefficient versus lift coefficient for M = 1 through 24.

In figure 24, it should be again assumed an infinite value for Cl at Mach 1. It is shown once again that higher attack angles have higher lift coefficients than lower attack angles.

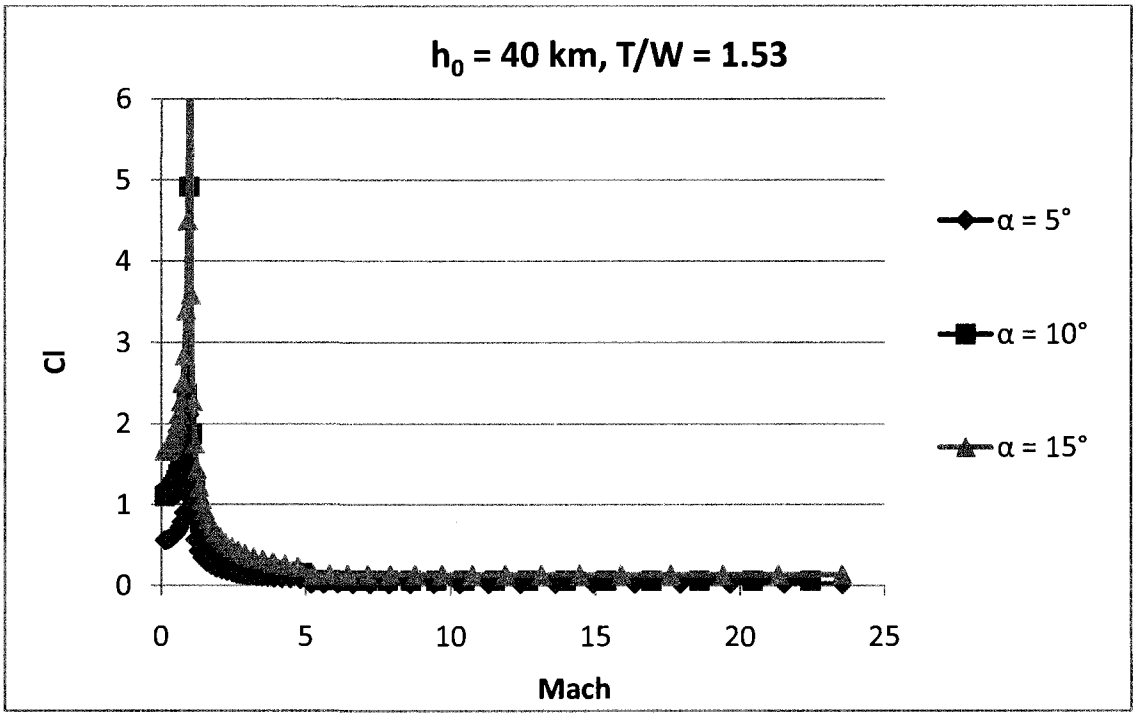

Figure 24. Mach number versus lift coefficient.

*Case 5: $h_0$ = 40 km, T/W = 5.1*

When comparing figure 25 to 16, a higher thrust to weight ratio will reduce the altitude required to travel to achieve the 8 km/s requirement. At higher attack angles, Mach 24 will be achieved in less trajectory distance than flying at lower angles. Figure 26 displays a close-up of the results for α = 5° to 15° in figure 25.

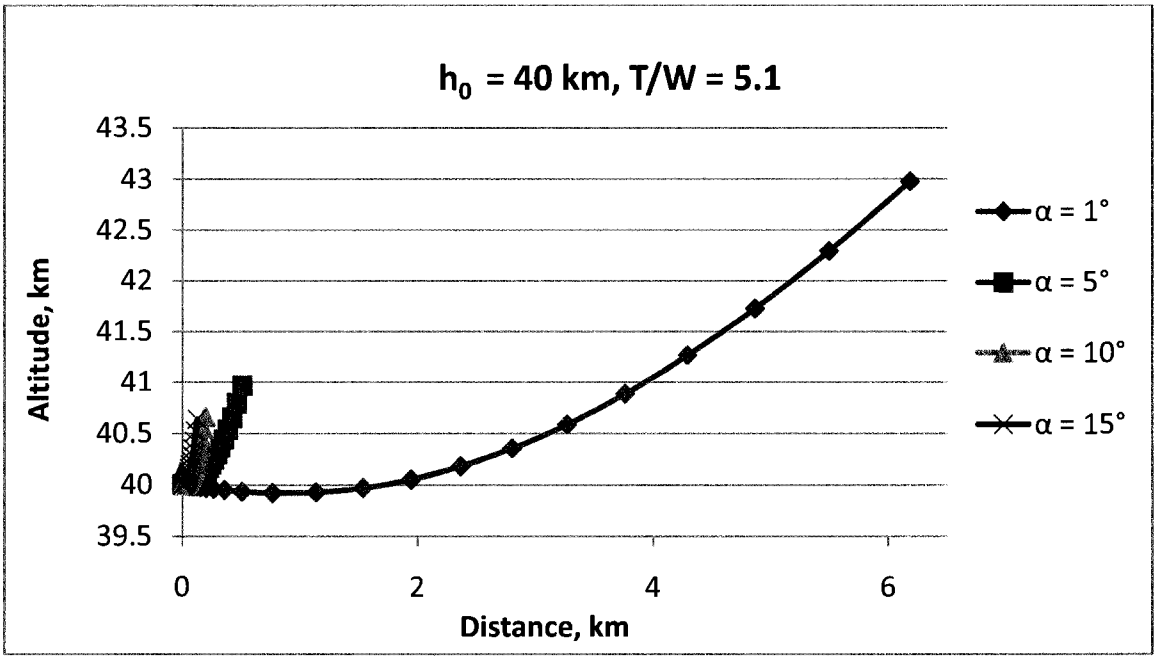


Figure 25. Distance versus altitude for $h_0$ = 40 km and T/W = 5.1.

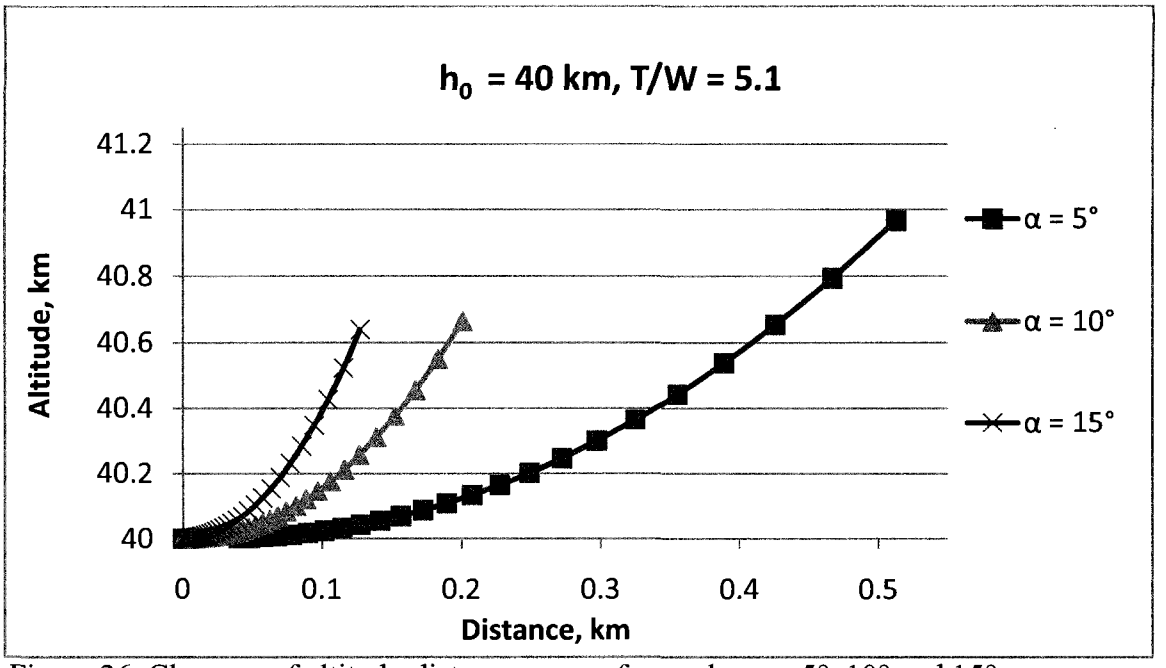

Figure 26. Close-up of altitude-distance curves for angles α = 5°, 10° and 15°.

Figure 27 shows how angles of attack of 5°, 10° and 15° result in the most stable velocity behavior while $\alpha = 1°$ presents an abrupt change at approximately Mach 13. Comparing to the 20 km launch results, the velocity behavior at $\alpha = 1°$ behaves more consistently during this lower altitude launch.

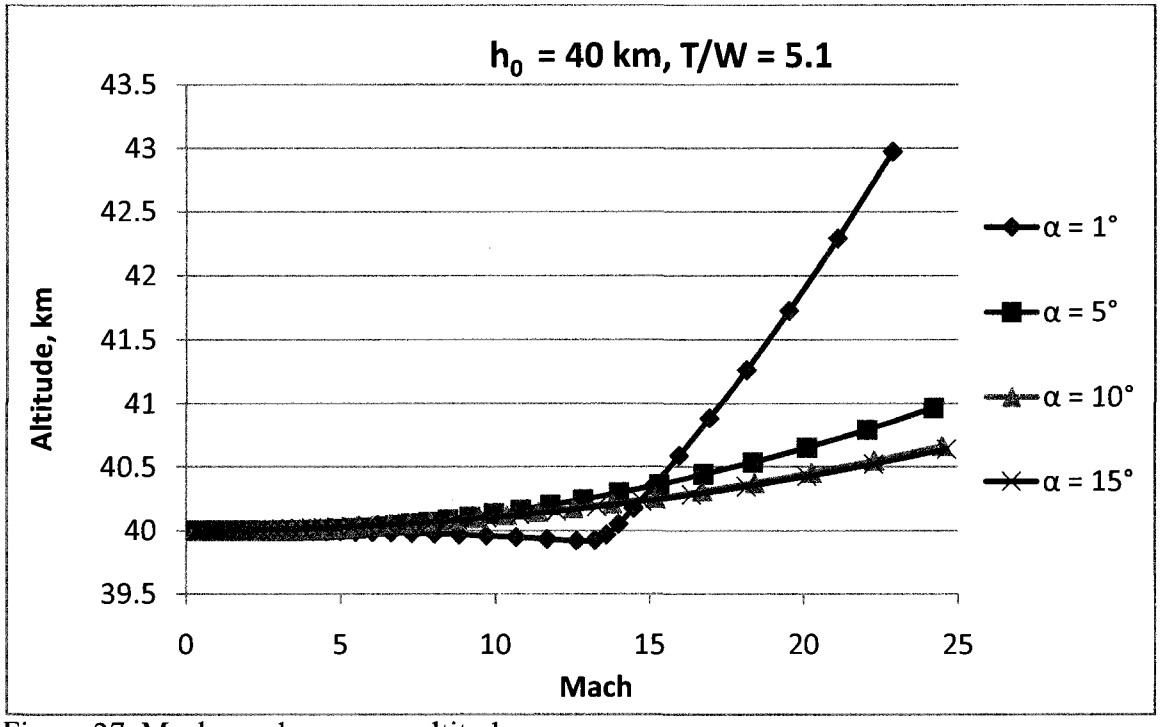

Figure 27. Mach number versus altitude.

Figure 28 displays Cl-Cd behavior for Mach 1 through 24. The higher the attack angle, the lower the Cl/Cd ratio.

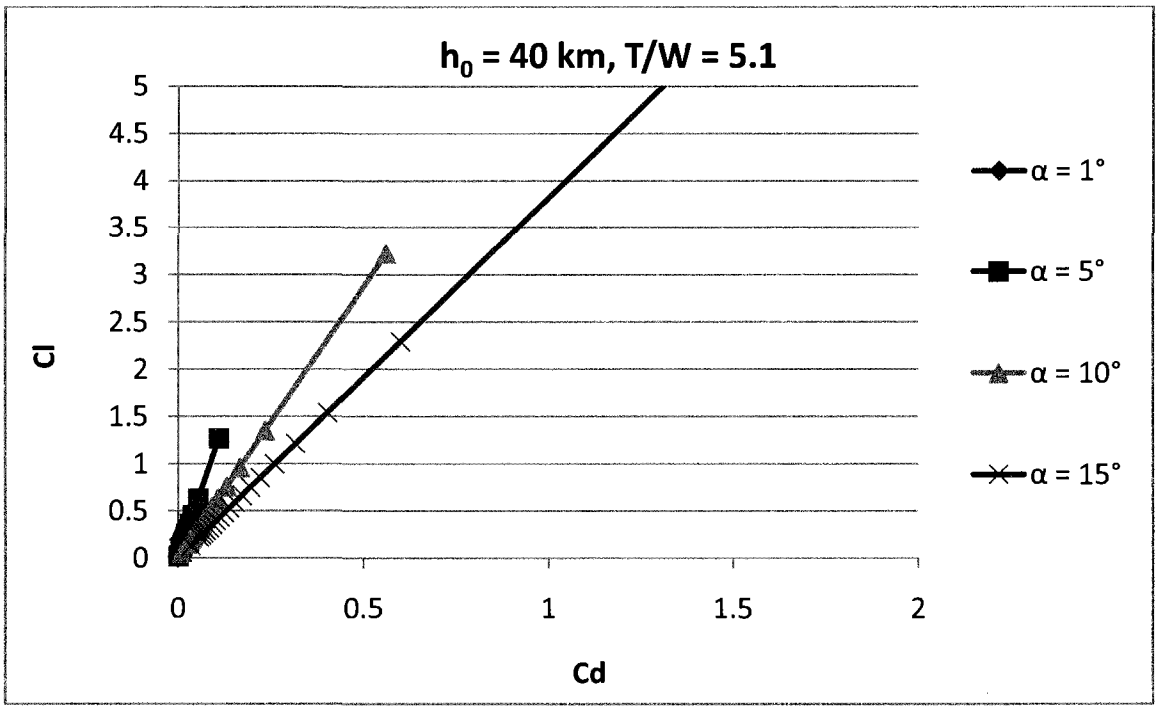


Figure 28. Drag coefficient versus lift coefficient for M = 1 through 24.

Figure 29 displays higher lift coefficients for higher attack angles versus lower angles as the Mach number increases.

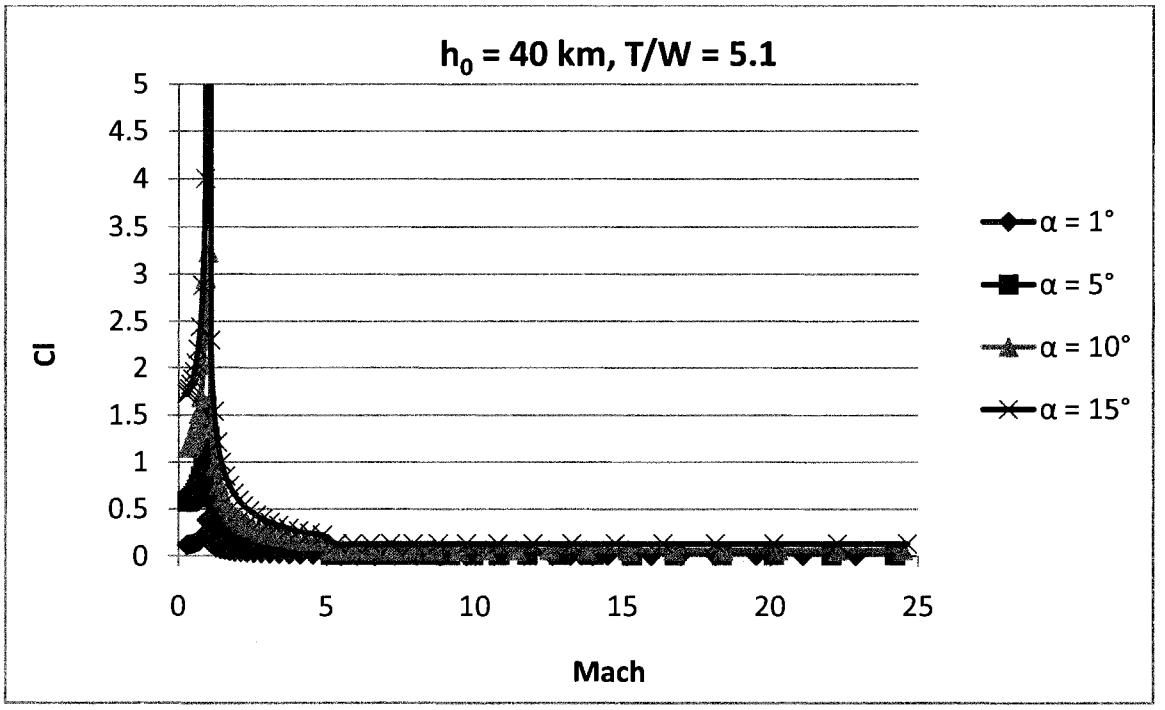

Figure 29. Mach number versus lift coefficient.

***Case 6: $h_0$ = 40 km, T/W = 10.19***

Comparing figure 30 to results at $h_0$ = 20 km, all attack angles result in a longer trajectory route from $h_0$ = 40 km to achieve its velocity requirement earlier. This is assumed to be due to lack of lift at this higher altitude.

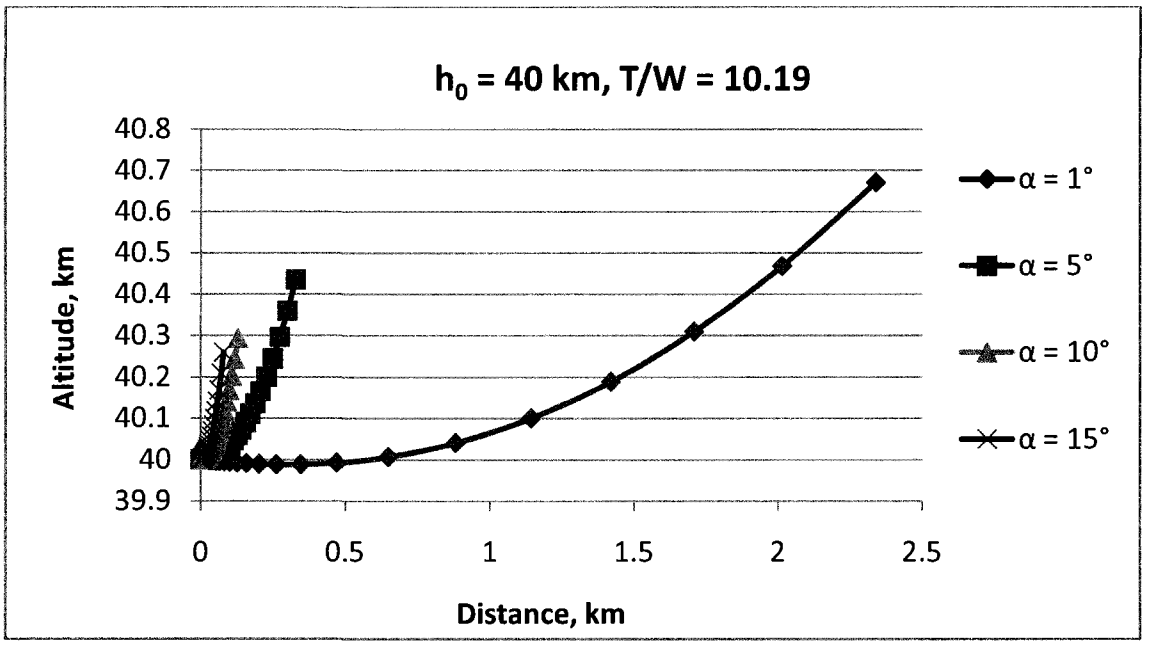


Figure 30. Distance versus altitude for $h_0$ = 40 km and T/W = 10.19.

Figure 31 displays how the results of an attack angle of 1° display an abrupt change at Mach 19 approximately increasing the change of rate in altitude. However, comparing to results lower T/W values (at $h_0 = 40$ km), there is less of an abrupt change for $\alpha = 1°$ results than before.

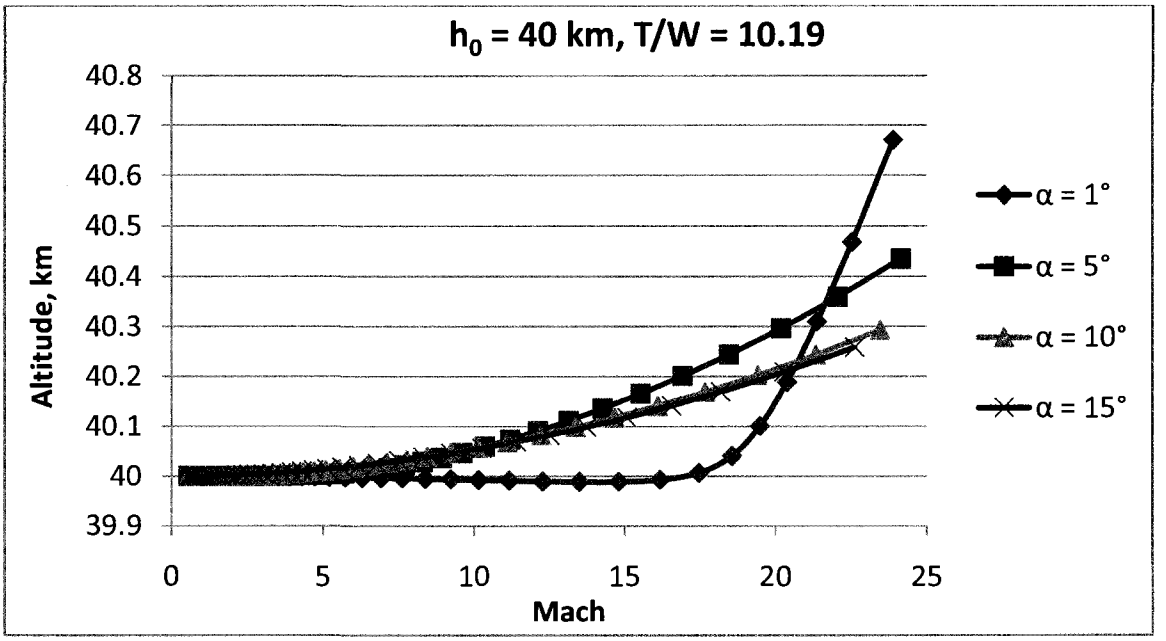

Figure 31. Mach number versus altitude.

Figure 32 displays the lower Cl/Cd ratio for higher attack angles. Figure 33 zooms into the results for $\alpha = 1°$.

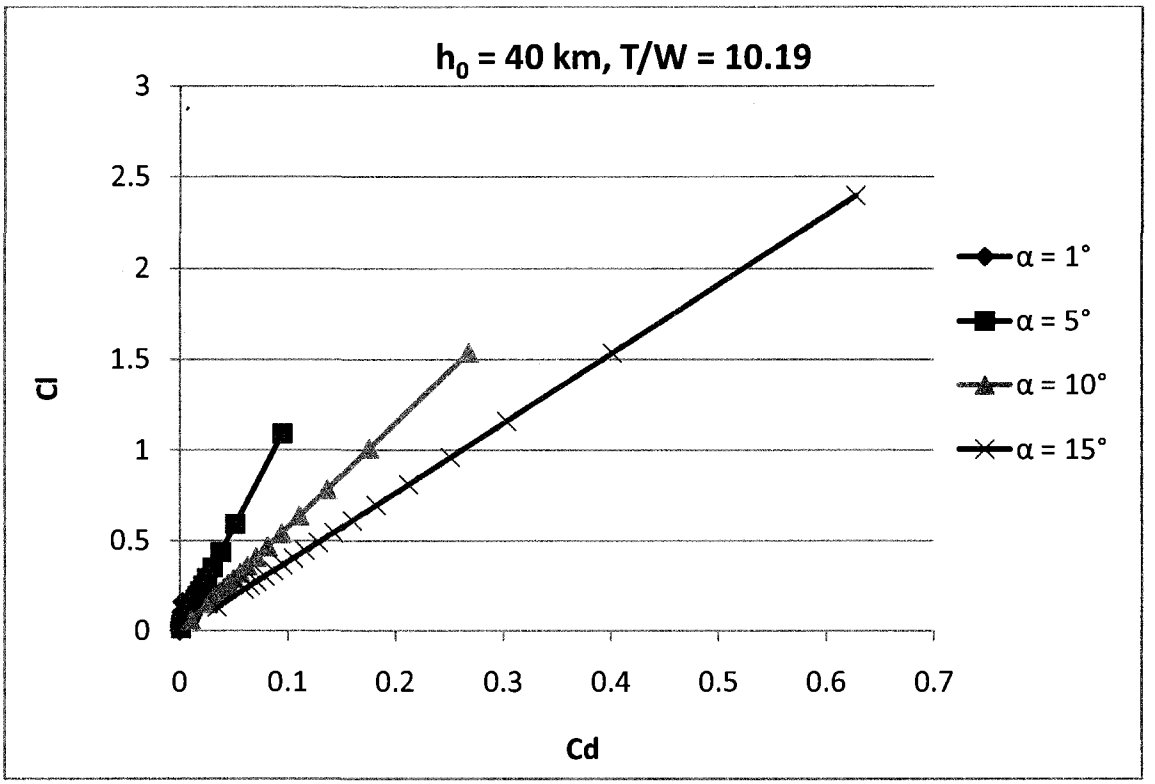

Figure 32. Drag coefficient versus lift coefficient for M = 1 through 24.

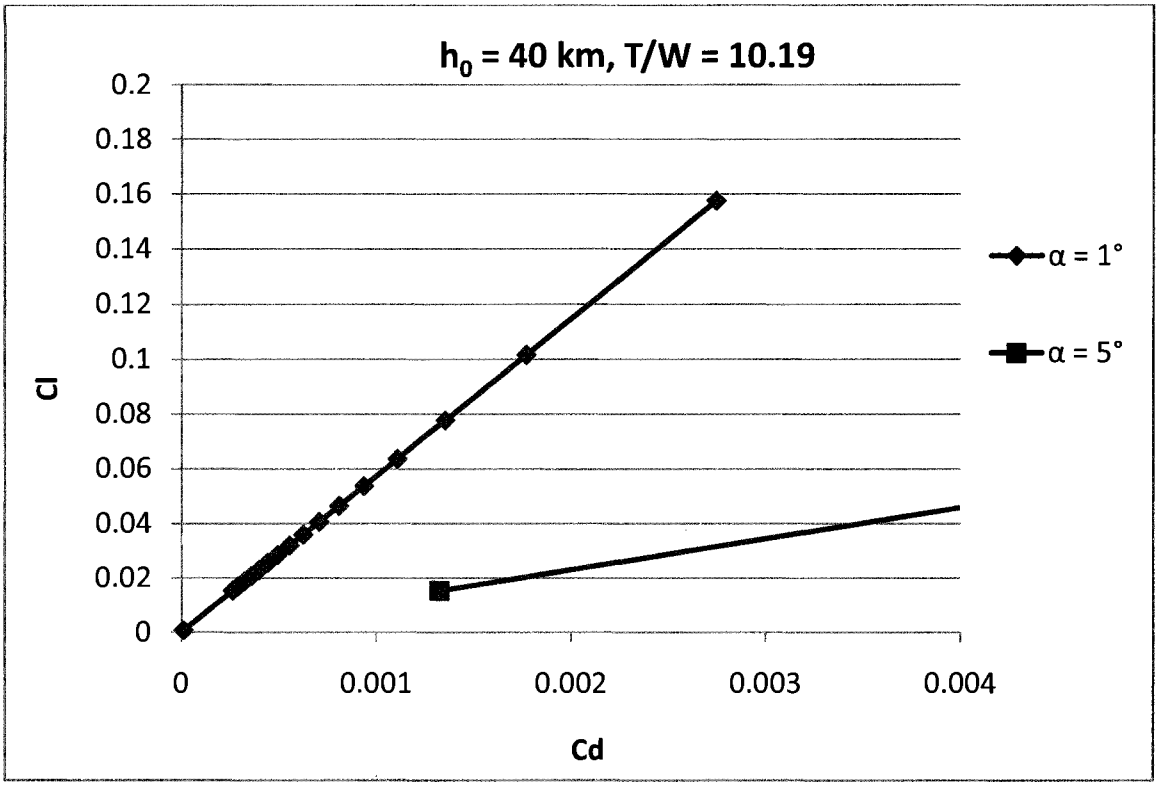

Figure 33. Drag coefficient versus lift coefficient for α = 1°.

Figure 34 demonstrates again the infinite Cl value at Mach 1. As shown higher angles of attack have higher lift coefficients than lower attack angles.

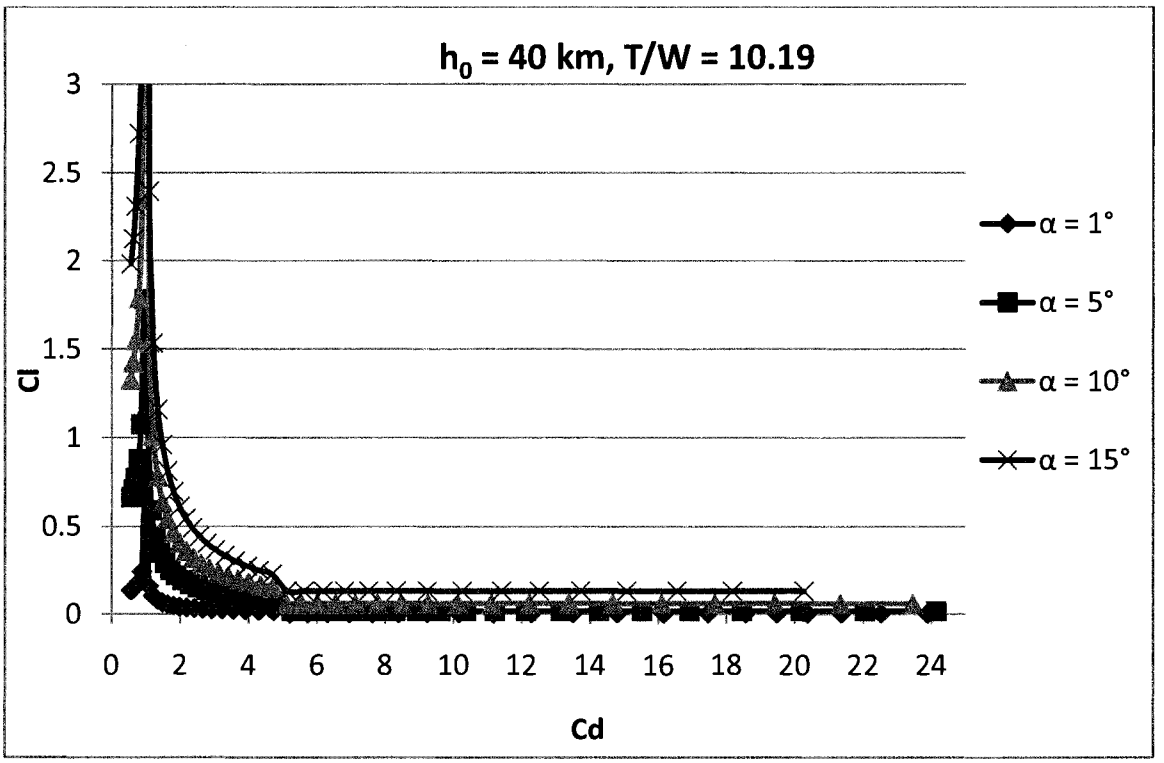

Figure 34. Mach number versus lift coefficient.

## Conclusions

When comparing all six cases, the first distinct difference was the wider range of angles of attack that the plate could be flown at when launching from the higher altitude of $h_0 = 40$ km.

In general, all the flight trajectories remained smoothest at higher T/W ratio. It was also observed that at $\alpha = 1°$ results were not favorable at low T/W ratios but improved with larger thrust values. When comparing only the results within one initial altitude, the higher the T/W ratio, the earlier the Mach of 24 was achieved.

When comparing results for different altitudes at constant T/W, a longer trajectory distance needed to be traveled to achieve Mach 24 at the higher initial altitude. This was due to less lift at higher altitude. The final altitude achieved however was nearly the same in both cases.

It was also observed that though higher angles of attack had more lift, they also resulted in lower Cl/Cd ratios than at lower angles of attack due to more drag.

To summarize the results and conclude this study, when comparing all six cases, a higher altitude with a high T/W ratio and a low angle of attack is preferrable.

## Appendix A: Particle Mean Velocity and Average Kinetic Energy Equations

The following integrals were necessary to use:

$$\int_0^\infty e^{-\beta x^2} dx = \frac{1}{2}\frac{\pi^{1/2}}{\beta^{1/2}} \tag{A.1a}$$

$$\int_0^\infty e^{-\beta x^2} x dx = \frac{1}{2\beta} \tag{A.1b}$$

$$\int_0^\infty e^{-\beta x^2} x^2 dx = \frac{1}{4}\frac{\pi^{1/2}}{\beta^{3/2}} \tag{A.1c}$$

$$\int_0^\infty e^{-\beta x^2} x^3 dx = \frac{1}{2\beta^2} \tag{A.1d}$$

$$\int_0^\infty e^{-\beta x^2} x^4 dx = \frac{3}{8}\frac{\pi^{1/2}}{\beta^{5/2}} \tag{A.1e}$$

The Maxwellian distribution is (Collie 313-319):

$$f(v)dv = A\, e^{-\beta v^2} v^2 dv\, d\cos\theta\, d\varphi \tag{A.2}$$

where $A$ is a normalization constant and $\beta = m/2kT$

Equating the integral of the distribution function to the particle density yields:

$$A = n\left(\frac{m}{2\pi kT}\right)^{1/2}$$

The mean velocity of particles in a half-space ( $\cos\theta > 0$ ) is obtained by:

$$n \cdot \overline{v_>} = 2\pi A \cdot \int_0^1 \cos\theta \, d\cos\theta \cdot \int_0^\infty dv \, v^3 e^{-\beta v^2} \tag{A.3a}$$

Therefore:

$$\overline{v_>} = \frac{1}{4}\bar{v} \quad \text{where} \quad \bar{v} = \left(\frac{8kT}{\pi m}\right)^{1/2} \tag{A.3b}$$

The average kinetic energy in the same half-space is given by:

$$n \cdot \bar{\varepsilon}_> = 2\pi A \cdot \int_0^1 \cos\theta \, d\cos\theta \cdot \int_0^\infty dv \left(\frac{m}{2} v^4\right) e^{-\beta v^2} \tag{A.4a}$$

Therefore (Anderson, *Hypersonic* 563):

$$\bar{\varepsilon}_> = \frac{3}{4} kT \tag{A.4b}$$

**Appendix B: MatLab Code**

```
unit.kg = 1.;
unit.km = 1.e+03;
unit.cm2= 1.e-04;
unit.cm3= 1.e-06;
unit.hr = 3600.;
unit.day = 24.*unit.hr;
unit.micron = 1.e-06;

Re_trans = 10^6;

rad_earth = 6.356766e+06;
rhoAir_0 = (28.e-03/6.023e+23)*2.687e+19/unit.cm3;
rhoMat = (27.e-03/unit.cm3)*100.*unit.micron;
pressure = 0.0;
spSound = 0.0;

g = 9.81;
mass = 500.*unit.kg;

Thrust = [7500.];
alfa_deg = [5.0];

for i = 1:size(Thrust)
   fprintf ('Thrust= %8.1f\n', Thrust(i));
   ToW = Thrust(i)/(mass*g);

  for j = 1 : size(alfa_deg)
      fprintf('Angle= %4.1f\n',alfa_deg(j));
      aoa_deg = alfa_deg(j);
      alpha = aoa_deg*pi/180.;
      Tx = Thrust(i)*cos(alpha);
      Ty = Thrust(i)*sin(alpha);
      figTitle = sprintf('trajectory for: T/W=%5.2f, alpha=%9.3f',ToW,aoa_deg);

      hconst = 40.0*unit.km; %scale constant for atmosphere model
      alt = hconst;

      % Additional constants:
      Pacc = 0.1; % For sigma = 0.36, in this case.
      A = 183.57
      k = 1.3806504*10^(-23); %J/K
```

```
sigma = 0.36;  % normally 5.6704*10^(-8);% W·m^-2·K^-4
Tmat = 473.15; % At 200 Celsius
v_bar = 0.25*(8*k*Tmat/(pi*mass))^0.5;

time = 0.0;
iter = 1;

step = 1.e-03;

V = [10.  0.];  %initial velocity
X = [0.  alt];  %initial position
trajT(1) = 0.;
trajX(1) = X(1)/unit.km;
trajY(1) = X(2)/unit.km;
trajU(1) = V(1);
trajV(1) = V(2);

figure(1)
title(figTitle);
plot(trajU,trajV,'.k');
xlabel('Vx (m/s)');
ylabel('Vy (m/s)');
M(iter) = getframe;

dVtot = 0.;
dLtot = 0.;
Vnorm = norm(V);
Lnorm = norm(X);

while(norm(V) < 9000.) %magnitude of speed

   sina = sin(alpha);
   cosa = cos(alpha);

   rhoAir = rhoAir_0*exp(-X(2)/hconst);
   r = (rhoAir/rhoMat);

   %Calculates variable density as a function of the alt
   R = 287; % N*m/(kg*K)
   h_geop = (rad_earth * X(2))/(rad_earth + X(2));

   if 0 <= h_geop  & h_geop <= 11000; % altitude, m
      T_1 = 288.16;
      h_1 = 0;
```

```
    h = h_geop;
    pressure_1 = 1.01325*10^5;
    %rhoAir_0 = 1.23;
    a = -6.5*10^(-3); %K/m
    T = T_1 + a*(h-h_1); %K
    rhoAir = rhoAir_0*(T/T_1)^(-g/(a*R)-1);
    pressure = pressure_1*(T/T_1)^(-g/(a*R));

elseif 11000 < h_geop & h_geop <= 25000; % altitude, m
    h = h_geop;
    h_1 = 11000;
    pressure_1 = 2.27*10^4;
    rhoAir_1 = 0.361;
    T = 216.66; %Kelvin
    rhoAir = rhoAir_1*exp(-g/(R*T)*(h-h_1));
    pressure = pressure_1 * (rhoAir/rhoAir_1);

elseif 25000 < h_geop & h_geop <= 47000; % altitude, m
    T_1 = 216.66;
    h_1 = 25000;
    h = h_geop;
    pressure_1 = 2.48*10^3;
    rhoAir_1 = 0.04;
    a = 3*10^(-3); %K/m
    T = T_1 + a*(h-h_1); %Kelvin
    rhoAir = rhoAir_1*(T/T_1)^(-g/(a*R)-1);
    pressure = pressure_1*(T/T_1)^(-g/(a*R));

elseif 47000 < h_geop & h_geop <= 53000; % altitude, m
    h = h_geop;
    h_1 = 47000;
    pressure_1 = 1.2*10^2;
    rhoAir_1 = 0.00148;
    T = 282.66; %Kelvin
    rhoAir = rhoAir_1*exp(-g/(R*T)*(h-h_1));
    pressure = pressure_1 * (rhoAir/rhoAir_1);

elseif 53000 < h_geop & h_geop <= 79000; % altitude, m
    T_1 = 282.66;
    h_1 = 53000;
    h = h_geop;
    pressure_1 = 5.8*10^1;
    rhoAir_1 = 0.000714;
    a = -4.5*10^(-3); %K/m
```

```
        T = T_1 + a*(h-h_1); %Kelvin
        rhoAir = rhoAir_1*(T/T_1)^(-g/(a*R)-1);
        pressure = pressure_1*(T/T_1)^(-g/(a*R));

    elseif 79000 < h_geop & h_geop <= 90000; % altitude, m
        h = h_geop;
        h_1 = 79000;
        pressure_1 = 1.2437;
        rhoAir_1 = 0.0000216;
        T = 165.66; %Kelvin
        rhoAir = rhoAir_1*exp(-g/(R*T)*(h-h_1));
        pressure = pressure_1 * (rhoAir/rhoAir_1);

    elseif 90000 < h_geop & h_geop <= 150000; % altitude, m
        T_1 = 165.66;
        h_1 = 90000;
        h = h_geop;
        pressure_1 = 0.18359;
        rhoAir_1 = 0.000003416;
        a = 4*10^(-3); %K/m
        T = T_1 + a*(h-h_1); %Kelvin
        rhoAir = rhoAir_1*(T/T_1)^(-g/(a*R)-1);
        pressure = pressure_1*(T/T_1)^(-g/(a*R));
    end;

    %speed of sound
    gamma = 1.4;
    spSound = sqrt(gamma * pressure/rhoAir);

    centrifug_acc = V(1)*V(1)/(rad_earth+X(2));

    fx = Tx-A*rhoAir*V(1)^2*(2*(1-Pacc)*sina^3+Pacc*sina+Pacc*sina^2*v_bar
/V(1));

    fy = Ty+mass*centrifug_acc-mass*g+A*rhoAir*V(1)^2*(2*(1-Pacc)*sina^2
*cosa+Pacc*sina*cosa*v_bar/V(1));

    step = r*(V(1)*V(1)+1.)/(1.+abs(V(2))+0.1*abs(V(1)));
    step = 0.03/step;
    dF = [fx*step;  fy*step];

    %predictor
    jac = [ 1.+2.*r*V(1)*sina*cosa*step     0.;
            -2.*r*V(1)*sina*sina*step     1.];
```

```
dV = (jac\dF)';
V1 = V + 0.5*dV;
dX = [V1(1)*step   V1(2)*step];
V = V1 + 0.5*dV;
X = X + dX;

time = time + step;

if(norm(V) >= 8000.)
   disp ' Success: Orbital velocity achieved! '
   break;
   %continue;
end

if(X(2) > 150*unit.km)
   disp ' In space now... '
   Vx = V(1)
   Vy = V(2)
   break;
   %continue;
end

if(X(2) < 0.)
   disp ' Crash and burn! '
   break;
   continue;
end

% check if plotting necessary
dVtot = dVtot + norm(dV);
dLtot = dLtot + norm(dX);
reldQ = max(dVtot/Vnorm,dLtot/Lnorm);

if (reldQ > 0.10)
   Vnorm = norm(V);
   Lnorm = norm(X);
   dVtot = 0.;
   dLtot = 0.;
   iter = iter+1;

   mach(iter) = norm(V)/spSound;
   trajT(iter) = time;
   trajU(iter) = V(1);
   trajV(iter) = V(2);
```

```
            trajX(iter) = X(1)/unit.km;
            trajY(iter) = X(2)/unit.km;
            x_forces(iter) = fx;
            y_forces(iter) = fy;
            density(iter) = rhoAir;
            plot(trajU,trajV,'-k');
            title(figTitle);
            xlabel('Vx (m/s)');
            ylabel('Vy (m/s)');

            M(iter) = getframe;
        end

        hf2 = figure('Name',figTitle,'NumberTitle','off');

        s1 = subplot(2,2,1);
        semilogy(trajT,trajY,'-k');
        xlabel('time (s)');
        ylabel('Altitude (km)');

        s2 = subplot(2,2,2);
        plot(mach, trajY, '-k');
        xlabel('Mach');
        ylabel('Altitude (km)');

        s3 = subplot(2,2,3);
        semilogy(trajT,trajU,'-k');
        xlabel('time (s)');
        ylabel('Vx (m/s)');

        s4 = subplot(2,2,4);
        plot(trajT,trajV,'-k');
        xlabel('time (s)');
        ylabel('Vy (m/s)');

        figure_name = sprintf('figure%d%d',i,j);
        %print -dpdf 'figure_name.pdf'
        print -dpdf 'figure2.pdf'
        %report trajectory.rpt

        fprintf('   Mach = %7.3f\n', mach);
    end % loop for angles
end % loop for thrust
```